Characteristics of Atmospheric Transport Using Three Numerical Formulations for Atmospheric Dynamics in a Single GCM Framework

PHILIP J. RASCH, DANIELLE B. COLEMAN, NATALIE MAHOWALD, AND DAVID L. WILLIAMSON

NCAR, Boulder, Colorado*

SHIAN-JIANN LIN

Geophysical Fluid Dynamics Laboratory, Princeton University, Princeton, New Jersey

BYRON A. BOVILLE AND PETER HESS

NCAR, Boulder, Colorado*

(Manuscript received 16 February 2005, in final form 31 August 2005)

ABSTRACT

This study examines the sensitivity of a number of important archetypical tracer problems to the numerical method used to solve the equations of tracer transport and atmospheric dynamics. The tracers' scenarios were constructed to exercise the model for a variety of problems relevant to understanding and modeling the physical, dynamical, and chemical aspects of the climate system. The use of spectral, semi-Lagrangian, and finite volume (FV) numerical methods for the equations is explored. All subgrid-scale physical parameterizations were the same in all model simulations.

The model behavior with a few short simulations with passive tracers is explored, and with much longer simulations of radon, SF_6, ozone, a tracer designed to mimic some aspects of a biospheric source/sink of CO_2, and a suite of tracers designed around the conservation laws for thermodynamics and mass in the model.

Large differences were seen near the tropopause in the model, where the FV core shows a much reduced level of vertical and meridional mixing. There was also evidence that the subtropical subsidence regions are more isolated from Tropics and midlatitudes in the FV core than seen in the other model simulations. There are also big differences in the stratosphere, particularly for age of air in the stratosphere and ozone. A comparison with estimated age of air from CO_2 and SF_6 measurements in the stratosphere suggest that the FV core is behaving most realistically.

A neutral biosphere (NB) test case is used to explore issues of diurnal and seasonal rectification of a tracer with sources and sinks at the surface. The sources and sinks have a zero annual average, and the rectification is associated with temporal correlations between the sources and sinks, and transport. The test suggests that the rectification is strongly influenced by the resolved-scale dynamics (i.e., the dynamical core) and that the numerical formulation for dynamics and transport still plays a critical role in the distribution of NB-like species. Since the distribution of species driven by these processes have a strong influence on the interpretation of the "missing sink" for CO_2 and the interpretation of climate change associated with anthropogenic forcing herein, these issues should not be neglected.

The spectral core showed the largest departures from the predicted nonlinear relationship required by the equations for thermodynamics and mass conservations. The FV and semi-Lagrangian dynamics (SLD) models both produced errors a factor of 2 lower. The SLD model shows a small but systematic bias in its ability to maintain this relationship that was not present in the FV simulation.

The results of the study indicate that for virtually all of these problems, the model numerics still have a large role in influencing the model solutions. It was frequently the case that the differences in solutions resulting from varying the numerics still exceed the differences in the simulations resulting from significant

* The National Center for Atmospheric Research is sponsored by the National Science Foundation.

Corresponding author address: Dr. Philip J. Rasch, NCAR, P.O. Box 3000, Boulder, CO 80307-3000.
E-mail: pjr@ncar.ucar.edu

physical perturbations (like changes in greenhouse gas forcing). This does not mean that the response of the system to physical changes is not correct. When results are consistent using different numerical formulations for dynamics and transport it lends confidence to one's conclusions, but it does indicate that some caution is required in interpreting the results.

The results from this study favor use of the FV core for tracer transport and model dynamics. The FV core is, unlike the others, conservative, less diffusive (e.g., maintains strong gradients better), and maintains the nonlinear relationships among variables required by thermodynamic and mass conservation constraints more accurately.

1. Introduction

As general circulation models (GCMs) have evolved, they have been used to examine increasingly ambitious and complex problems and the quality of their simulations have been held to an increasingly high standard. Many problems being addressed today require careful formulations of transport of constituents as one component of the model framework that comprises a GCM.

The movement of a field from one location to another appears in equations governing most physical processes represented in a GCM. Sometimes it is a dominant term in the physics. Frequently, it appears as one term among a few that are important in controlling a physical process. It is also frequently the case that it is possible to identify errors (occasionally large) in the numerical solution that arise from the formulation for transport, either by processes explicitly resolved by the model, or those unresolved processes that must be parameterized in a model. It is thus important to try to reduce those numerical errors so that they are small compared to the terms associated with the physics of the problem.

It is difficult to design a numerical algorithm that is accurate, computationally efficient, and sufficiently general that it will handle the broad scope of problems required of it in a GCM. In our experience, it is possible to identify numerical artifacts that arise from mixing different numerical methods for treating advective processes. Therefore, it is desirable to use the same algorithm for atmospheric transport in all model variables represented in a model, yet those variables have different physical characteristics and vary over disparate time and space scales.

These issues of transport are intimately tied to the formulation for the dynamical equations of motion as well. Advection appears as one of the important terms in those equations, and transport is obviously dependent on the wind fields that arise from the solutions with the equations of motion.

A variety of techniques have been developed in the climate modeling community for solutions to atmospheric transport, and some of these techniques have been used in the development of the National Center for Atmospheric Research (NCAR) Community Climate System Model (CCSM). Originally, in the Community Climate Models CCM0, CCM1, and CCM2, a combination of spectral and finite difference (FD) methods were used in the transport of water vapor, and the dynamical variables expressed temperature and momentum (Williamson 1983). Later, for CCM2, a semi-Lagrangian transport formulation was added for water vapor and other trace species, but the dynamical variable transport was spectral (Williamson and Rasch 1994; Rasch and Williamson 1990). This produced an inconsistent formulation, but it was still an improvement compared to the pure spectral/FD formulation. Subsequently, Williamson and Olson (1994) developed a complete semi-Lagrangian dynamics' formulation in which the transport terms for both dynamical variables and trace constituents were handled consistently and uniformly. Recently, a new dynamical framework was developed by Lin (2004) using a control volume formulation. It also treats the dynamical variables and trace constituents uniformly and more consistently than the spectral cores discussed here.

Transport problems in GCMs can be attributed to errors in three model aspects: Errors in the numerical methods used to solve the differential equation describing tracer transport; transport errors arising from biases in the wind and mass fields themselves that are a result of problems with the general circulation of the model; and transport errors resulting from errors in subgrid-scale parameterizations.

This paper focuses on the first two components of this list, namely, errors introduced from numerical discretizations of the tracer transport equation, and errors arising from the solutions to equations describing the general circulation. Errors from the third model component (the parameterizations) are still present, but the fundamental formulation of the parameterizations is constant across the range of model cases explored here. The response of Community Atmosphere Model's (CAM) tracer transport to variations in the formulations for tracer transport and atmospheric dynamics processes and to model resolutions is examined in a number of archetypical trace-constituent transport

problems. Each of the test problems were chosen to illustrate the behavior of the model for a different class of trace constituents, each of which is representative of a broader class of constituents. The use of test tracer problems for understanding both model biases and atmospheric processes has a long history in the chemistry and climate communities. It is impossible to cite all of the important work in this area, but many important studies are outlined and cited in Prather and Remsberg (1992), Boville et al. (1997), Pyle and Prather (1996), Jacob et al. (1997), and Rasch et al. (2000) for chemistry; and in Rind and Lerner (1996) and Rind et al. (1999), which, as in other papers cited here, suggested the use of tracers as a diagnostic tool in GCM development.

While many of these problems have been used before in the literature, we are not aware of their examination in a context in which all processes except the tracer transport and dynamical formulation are identical, and all model configurations have been constructed to produce approximately the same climate in the context of seasonally and annually averaged temperature, radiation, and wind fields. We have also examined the sensitivity of the tracer solutions to changes in model climate induced by anthropogenic forcing (e.g., Butchart and Sciafe 2001; Rind et al. 2001; Collins et al. 2003; Zeng and Pyle 2003).

Lastly, we acknowledge that we are necessarily brief in our discussion of each tracer, and have restricted our discussion to zonal and annual averages. It would have been possible to explore and discuss the simulations with decompositions including seasonal, and latitudinal/longitudinal information, but that would have necessarily produced a much different and longer paper.

2. Brief description of CAM3

Since a description of components of CAM3 can be found in other papers appearing in this special issue, we point the reader to the relevant papers describing these components, and highlight issues that influence the variability of the model simulation of tracers.

A general overview of the CAM3 is provided in Collins et al. (2006b). CAM can be used as a stand-alone atmospheric general circulation model, or as a component of a climate system model that includes formulations for the physical, chemical, and biological evolution of ocean, sea ice, and land components of the earth system (Collins et al. 2006a). CAM can be run at varying resolutions, and can use varying numerical formulations for atmospheric dynamics and transport. Three formulations are supported for the representation of atmospheric dynamics and transport, generally referred to as a dynamical core. The standard dynamical core uses the classic spectral method for representing the evolution of the equations of motion. It combines a transform method employing spherical harmonics for horizontal discretizations, with nominally second-order finite differences for the vertical discretization for the equations of motion. Because the spectral method is not suitable for constituent transport (Rasch and Williamson 1990, 1991) a semi-Lagrangian method is employed for representing the evolution of trace-constituent mixing ratios (Williamson and Rasch 1994). The different numerical methods exacerbate inconsistencies between the model wind fields, the transport of air masses and tracers, and fixers that are required to produce a formulation that conserves tracer mass (Williamson and Olson 1994; Rasch et al. 1995). CAM3 also includes a semi-Lagrangian dynamics (SLD) core (Williamson and Olson 1994; Collins et al. 2004), where more terms in the equations of motion and constituents are treated consistently using the semi-Lagrangian framework. This improves the consistency of the transport formulation, and results in a model framework that may be more advantageous for constituent transport. However, the model still requires the previously cited fixers. The third option for a dynamical core is a finite volume discretization following Lin (2004). This formulation expresses all evolution equations in flux form, resulting in a fully conservative formulation, with improved consistency in the framework for the dynamics and constituent transport.

All versions of the model use the identical formulation for the physical parameterizations, and have been tuned to produce simulations that are energetically balanced and are quite similar in their seasonal and annual features of the general circulation. Some of the model simulation used a slab ocean model (SOM) formulation that includes a simple representation for the ocean mixed layer and a thermodynamic sea ice component based on the CCSM3 sea ice model, with the implied ocean heat-transport calculated from a stand-alone control version of CAM. The SOM provides a mechanism for exploring the response of the atmosphere to changes in radiative forcing in a simpler context than the fully coupled model (Kiehl et al. 2006). To identify differences in transport, we have also run the CAM–SOM with preindustrial as well as future climate change scenarios, as described in Otto-Bliesner et al. (2006) and Kiehl et al. (2006). When run with present-day radiative forcing, the SOM and stand-alone model simulations are virtually indistinguishable, both in terms of the general circulation and in terms of the tracer distributions described here. The models also do differ somewhat in their representation of transient features

TABLE 1. The cases examined in this study, ordered from lowest to highest resolution. Note that although the semi-Lagrangian and spectral T42 models contain the same number of grid points, the former model does not use the inherent smoothing required for a spectral transform model.

Case	Resolution	Dynamics	SST	Time step (s)
T42amip	128 × 64	Spectral/FD	Prescribed 1950–54	1200
T63SLDamip	128 × 64	Semi-Lagrangian/FD	Prescribed 1950–54	3600
FVamip	144 × 91	Control volume	Prescribed SST	1800
T42som-present	128 × 64	Spectral/FD	Predicted SST	1200
T42som-past	128 × 64	Spectral/FD	Predicted SST	1200
T42som-future	128 × 64	Spectral/FD	Predicted SST	1200

(Rasch et al. 2006) of the hydrological cycle. We have explored the simulation of these atmospheric trace constituents for six different model configurations described in Table 1.

All model versions (with the exception of the simulations described in section 3a) were started at near equilibrium conditions and were run for ten years. The versions of the model identified as having a 128 × 64 resolution have horizontal cell dimensions of approximately 2.8° on a side. The FV model employs a 2° × 2.5° regular latitude/longitude grid with cell centers located at poles and equator. There are approximately 60% more points on the globe than the 128 × 64 grid model configurations.

3. Simulations

We have explored the model behavior for a variety of trace constituents. These tracers characterize different aspects of transport. The suite provides a much broader overview of transport in each model than any individual constituent simulation, and frequently the behavior of one of the tracers helps in interpreting the behavior of another.

a. Passive tracers with high gradients

We begin by exploring the differences in transport properties in the model using two passive tracers (hereafter LOW, and HIGH), initialized to unity in a single model layer (near 800 and 200 hPa, respectively), and zero elsewhere (see Fig. 1). Each model used initial meteorological conditions for 1 September from an arbitrary year of a previous simulation, and was run for 30 days. The LOW tracer provides an indication of transport in a region of the atmosphere strongly influenced by subgrid-scale transport processes (e.g., convection and turbulent boundary layer processes). The HIGH tracer, particularly in middle and high latitudes, is much less strongly influenced by subgrid-scale processes with a larger role being played by resolved-scale dynamics.

Snapshots at day 15 and day 30 are shown for the LOW tracer initialized near the surface in Fig. 2. Each model configuration shows similar features: a relatively rapid mixing between the surface and tropopause in the Tropics, low values of the tracer in the subtropical subsidence regions, and a broader structure of mixing in midlatitudes and polar regions. In the subtropics, isolines of tracer tend to align with isentropes, a result of the relatively slow, cross-isentropic transport, and more rapid along-isentrope transport occurring in this region. A closer examination reveals quantitative differences between the various model simulations. At day 15, one sees air with lower concentration of tracer LOW in the subtropics in the FV simulation, characteristic of air originally of mid- and upper-tropospheric origin and the gradient between Tropics and subtropics is steeper. At day 30, these features are also evident. The gradient between low and high mixing ratio air in the subtropics is about a factor of 2 higher in the FV core than either of the other two configurations. At this time of year, mixing is more rapid in the Southern Hemisphere extratropics than in the Northern Hemisphere in all model configurations.

The features seen in the LOW tracer subtropics are also seen in the HIGH tracer concentration in the subsidence regions of the subtropics. The high concentration region is more coherent in the FV model than the other two dynamical core configurations. This is most evident on day 15, but also in evidence in at day 30.

The most striking feature of the HIGH tracer (Fig. 3), is the substantial difference in mixing in the upper-tropospheric polar region between the FV core and the spectral and semi-Lagrangian cores. The FV core has preserved the initial gradient much more strongly than the other cores. Note for example the 0.01 contour at day 30 (the isoline delimiting the white and gray regions of the figure). This isoline is located between 300 and 400 hPa in the FV model and between 600 and 800 hPa in the other two models. The extent of the region with mixing ratios exceeding 0.5 extends to within 35° of the equator in the FV model and is restricted to much

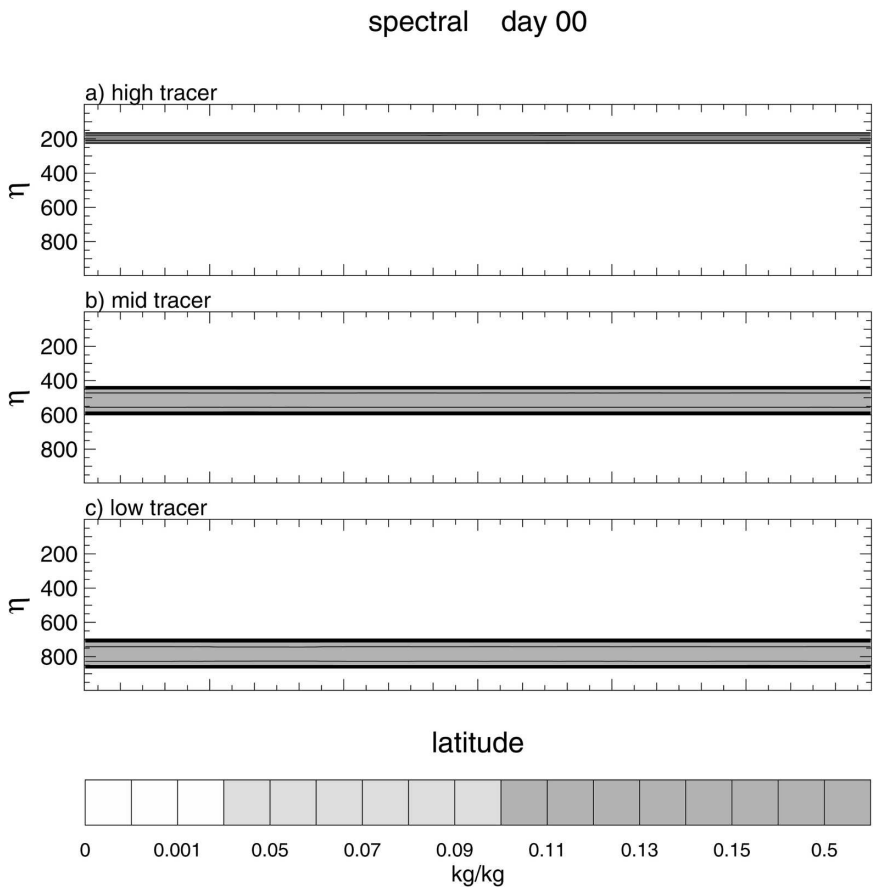

FIG. 1. Initial conditions for (a) HIGH, (b) MID, and (c) LOW tracer.

smaller regions poleward of about 60° in the other two models. There are also significant differences in the lower tropospheric polar regions. While the contours of Fig. 3 are linear in the light and middle-gray shaded regions of the figure, they are approximately logarithmic in the white and dark-gray shaded regions of the figure. In light of this, one can see that the concentration near the surface is a factor of 2 to 4 lower in the FV core than either of the other two cores, highlighting the reduced vertical mixing in the FV core. Simulations using tracer MID produced results consistent with the LOW and HIGH tracers; for this reason we have omitted a discussion of those results.

b. Radon

Radon has many virtues as a tracer of air recently at the surface (e.g., Liu et al. 1984). It has a short radioactive lifetime (half-life of 3.8 days), is thought to have a relatively uniform source, has low reactivity with other atmospheric constituents and is insoluble. Its main disadvantage is that it occurs at very low concentrations in air (mixing ratios of order 1 part in 10^{20}) and so direct measurements are difficult to make rapidly. Nevertheless it has frequently been used as a metric for evaluating atmospheric models (Feichter and Crutzen 1990; Jacob and Prather 1990; Genthon and Armengaud 1995; Jacob et al. 1997; Rasch et al. 2000)

We have employed a relatively standard scenario for our radon simulations (see, e.g., Jacob et al. 1997) by employing uniform emissions of 1 atom cm^{-2} s^{-1} over all land masses equatorward of 60°. The model runs were initialized with a concentration of zero, run for 10 yr, and averaged for the last 5 yr to produce the diagnostics used here.

Figure 4 shows some zonally averaged results. Because of the very strong stratification of radon with altitude (see bottom center panel showing the spectral T42 simulation), and the relatively small differences in the simulation, we have chosen to compare the simulations in terms of the ratio of zonal averages for each case with respect to the spectral T42 simulation. The upper left panel shows the ratio of the SLD simulation to the control; 20%–30% more radon is seen in the upper troposphere in the SLD simulation. As will be

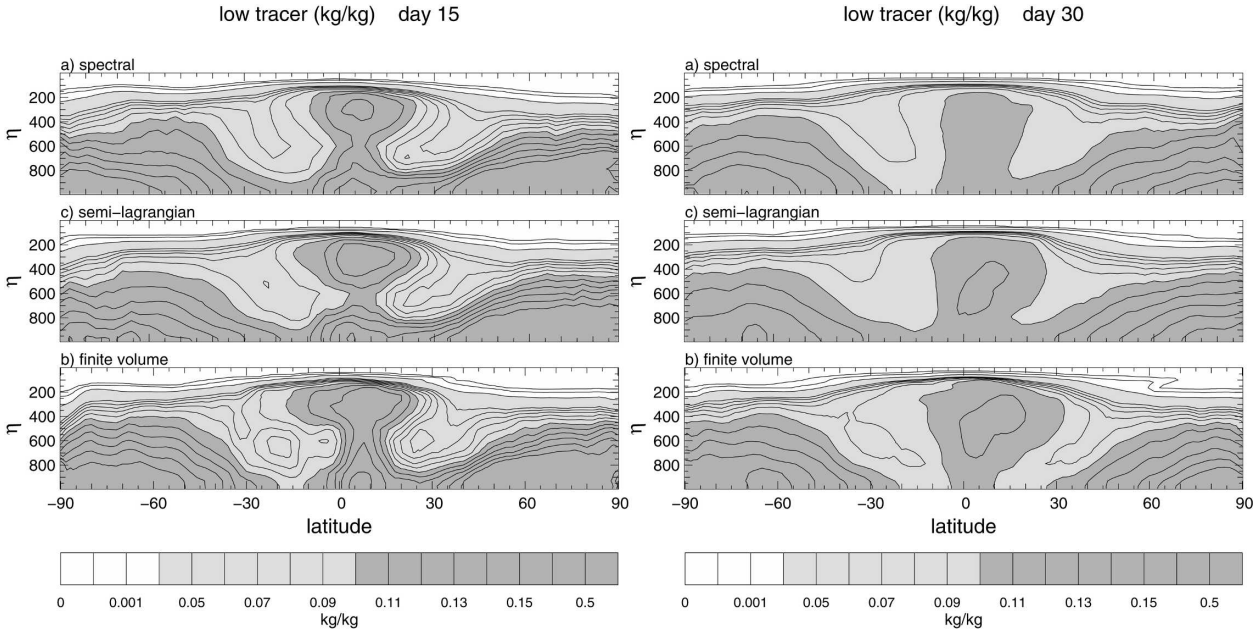

FIG. 2. Zonal averaged mixing ratio for days (left) 15 and (right) 30 for LOW tracer: (a) spectral, (b) semi-Lagrangian, and (c) finite volume.

seen in other tracers, this signature is consistent with a reduced cross-tropopause exchange of the SLD compared to the spectral core. Less transport of radon into the stratosphere results in higher concentrations in the troposphere. The ratio of radon in these two simulations drops to 0.4 as one approaches the model top, suggesting that transport processes operate more slowly in the SLD core than the spectral core in the stratosphere. There is little difference in the middle and lower troposphere between these two cases, where mixing is quite rapid and strongly controlled by the subgrid-scale parameterizations.

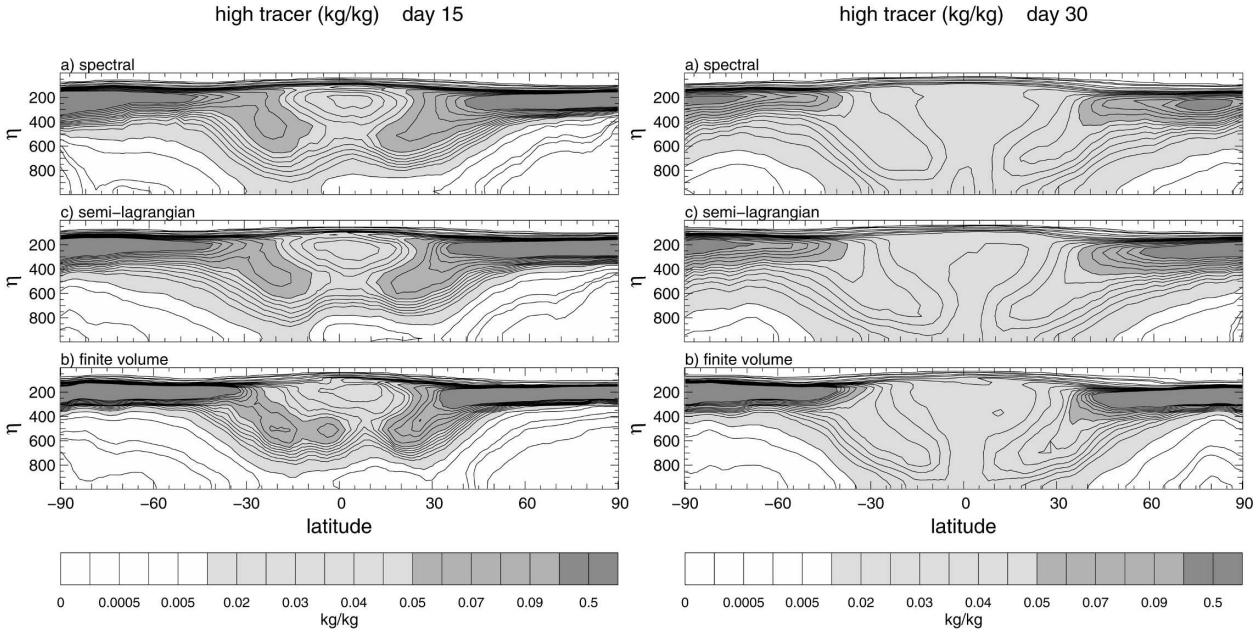

FIG. 3. As in Fig. 2 but for HIGH tracer.

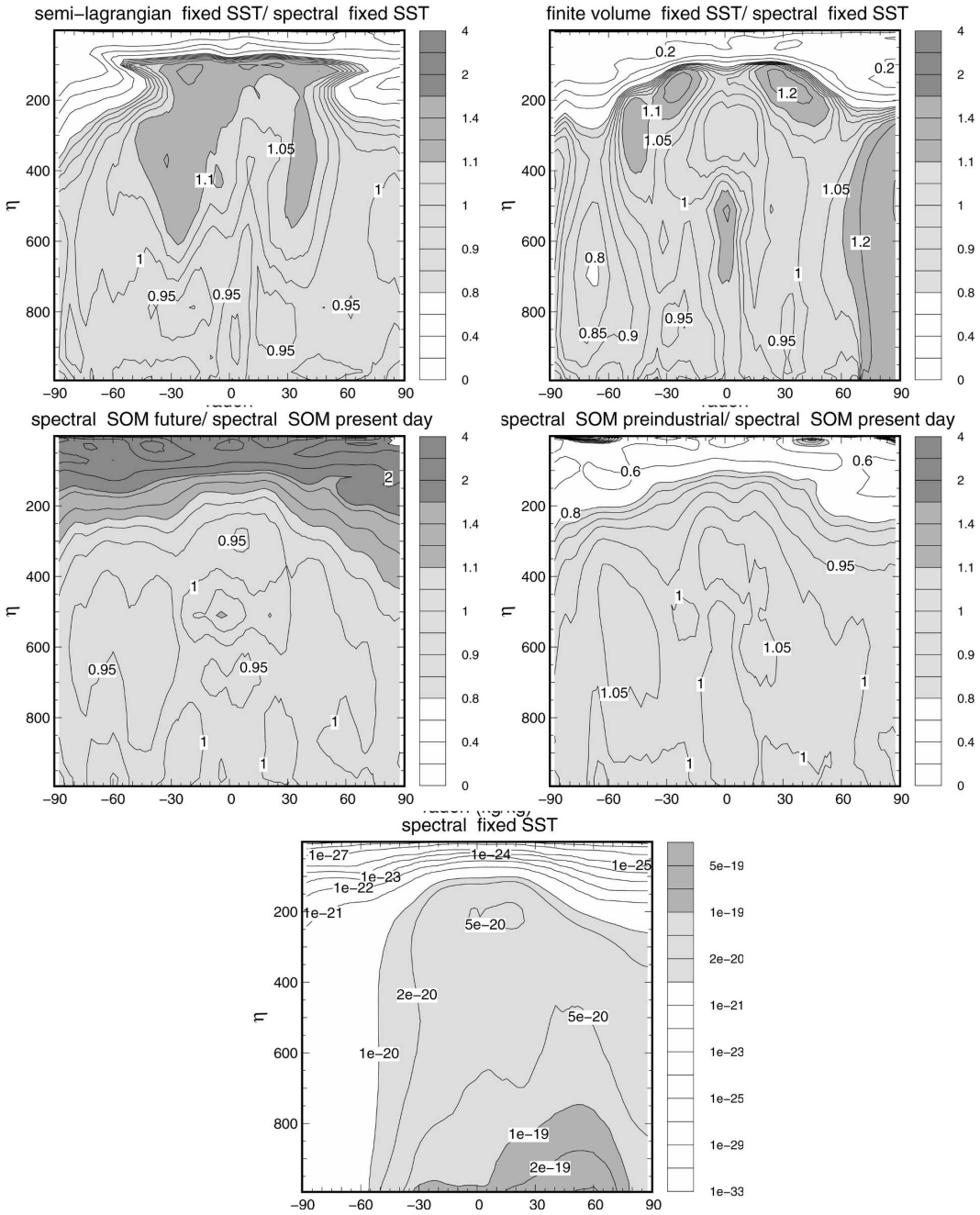

FIG. 4. Zonal averaged mixing ratio of radon for (bottom) the spectral T42 run and (top four panels) ratio of various cases to that run. Changes in shading indicate that the contour interval has changed.

The distinct differences seen in the polar regions at the tropopause in the SLD simulations can be explained by the temperature difference between the two simulations shown in Fig. 5. The SLD simulation is warmer, closer to the observed temperature distribution, and substantially reduces a known bias in the spectral T42 simulations (Williamson and Olson 1998). The warmer temperatures stabilize the vertical profile in that region and thus act to suppress any intrusions of tropospheric air carrying radon in the region.

The upper right panel of Fig. 4 shows the ratio of the zonal averages of radon between the FV and T42 simulations. Concentrations are again enhanced below the tropopause in the FV model compared to the SLD simulations, and reduced above it. The enhanced region of the upper troposphere is somewhat smaller than that

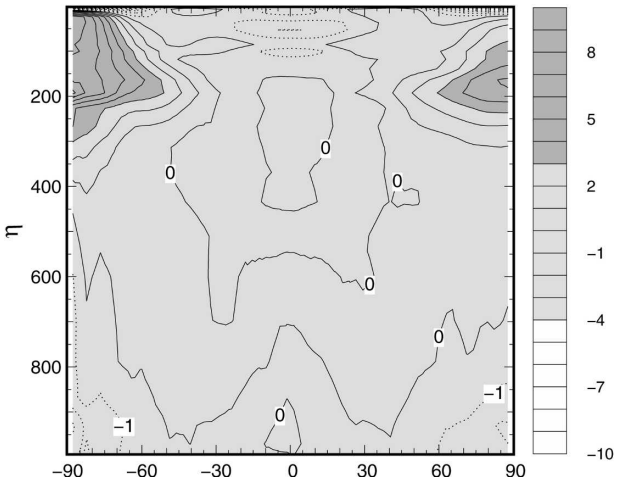

FIG. 5. Zonal average of the temperature difference between the SLD simulation and the spectral T42 simulation (units: K).

seen in the SLD core simulation. The depleted region in the stratosphere reaches even lower ratios (<0.2) than the SLD simulation. There is also significantly more radon in polar regions throughout the depth of the troposphere in the FV model, implying a more rapid exchange of tropospheric air between midlatitudes and polar regions.

The two central panels show ratios of zonal, annually averaged radon when transported in a model framework simulating the atmospheric response to changes in radiative (aerosol and greenhouse gas) forcing between a preindustrial, present-day, and future world. The model shows an increase in exchange of air between the troposphere and stratosphere. Radon is higher by a factor of 2 in the stratosphere in the future simulations compared to present day, and lower by about the same amount in the preindustrial simulations. This signal is consistent with the simulations of Butchart and Sciafe (2001), Rind et al. (2001), Collins et al. (2003), and Zeng and Pyle (2003), who demonstrated a general increase in stratosphere–troposphere exchange (STE) (both upward in the Tropics, and downward in midlatitudes) as a result of a general increase in the residual mean circulation in a world experiencing forcing from doubled CO_2. But it is clear that the numerical solution technique can easily influence the simulation at a level that can strongly modulate the physical signal of interest.

c. *Age of air and SF_6*

It is instructive to next contrast a relatively short-lived species with a continental surface source like radon with a constituent that has a very long lifetime, and a surface source. One such tracer is sulfur hexafluoride (SF_6), which has a lifetime of >1000 yr, is believed to be slowly emitted from electrical switching equipment (with a dominant source in the Northern Hemisphere), and is estimated to have had a nearly linear increase in emission rate. It has provided a useful measure of mixing between continental and maritime regions (Denning et al. 1999), of hemispheric exchange, and of exchange processes between the troposphere and stratosphere and within the stratosphere itself (Hall and Plumb 1994; Hall et al. 1999; Eluszkiewicz et al. 2000; Waugh and Hall 2002).

Emissions of SF_6 were prescribed using the inventories of Babiker et al. (2001). The model runs were initialized with a mixing ratio of zero pptv everywhere, and integrated for 10 yr. The figures in this section are the result of analyzing the last 5 yr of these simulations.

Figure 6 shows the zonal and annual average of SF_6, and case ratios following the conventions described for Fig. 4. The lower panel uses units of mass mixing ratio. Although it cannot be inferred from the regular contour interval chosen for the Figure, the pole to pole gradient in volume mixing ratio (mole fraction) units is about 0.35 pptv, in reasonable agreement with the composite analysis of the observations produced in The Atmospheric Tracer Transport Model Intercomparison Project (TRANSCOM II) study of Denning et al. (1999), and agreement with the group of models with stronger latitudinal gradients documented in that study. At northern midlatitudes, near the major emission regions for SF_6, the vertical gradients between the surface and 200 hPa are about 15%, again in agreement with the group of models having a relatively strong vertical gradient compared to the ensemble mean. The dominant, interhemispheric transport occurs in the middle and upper troposphere as indicated by the protrusion of higher mixing ratio air there and a weak, reversed gradient of SF_6 with higher mixing ratios aloft near the equator.

There is little quantitative difference in distributions in the troposphere as modeled by the different dynamical cores (upper two panels of Fig. 6), with differences of less than 2% between them. The FV model tends to export SF_6 slightly more rapidly from the Northern Hemisphere source region than the spectral model, while the SLD model exports slightly less. SF_6 tends to accumulate in higher mixing ratios in the upper troposphere, and both the FV and SLD cores transport less SF_6 into the stratosphere than the spectral model. The middle panels of Fig. 6 show the same signature in STE as the radon analysis. As anthropogenic forcing increases, transport into the stratosphere increases. The interhemispheric gradient is enhanced with increasing forcing, again consistent with the results of Rind et al. (2001), who found a similar signal in the Goddard Institute for Space Studies (GISS) model.

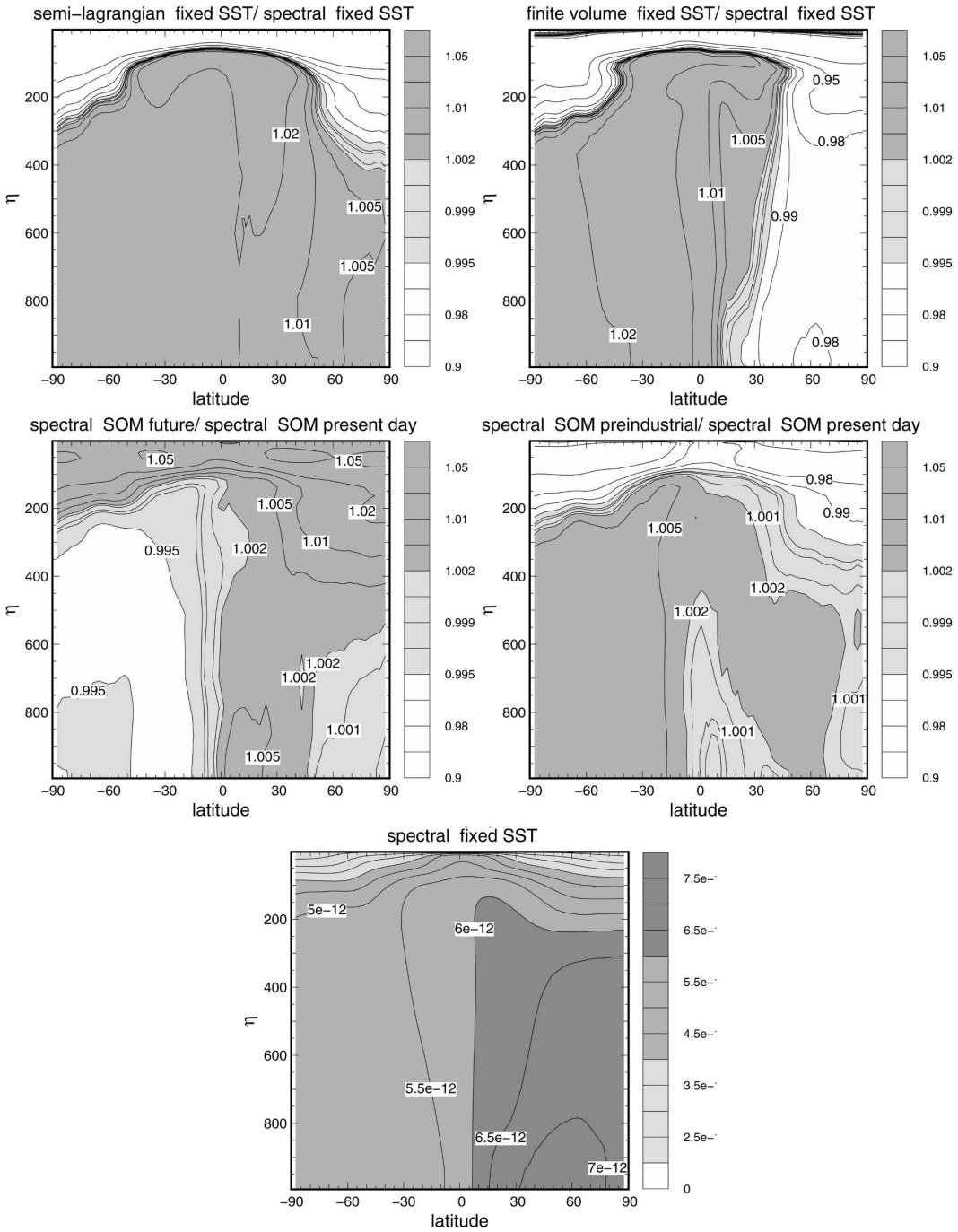

FIG. 6. Zonal averaged mixing ratio of SF_6 for the spectral T42 run. Lower panel has units of mass mixing ratio. Top four panels show the ratio of various cases to that run using dimensionless units.

A useful diagnostic of transport from the troposphere to the stratosphere is some measure of the elapsed time that it takes for fluid parcels to reach a given location in the stratosphere from the tropical tropopause. This quantity is really an integral of the age of air of many parcels traveling by different trajectories to a given location, and represents a type of Green's function that propagates the information at the tropical tropopause into the stratosphere. A recent review of this topic, with citations for a large body of the original literature, can be found in Waugh and Hall (2002). The age of air can be calculated a number of ways. One easy

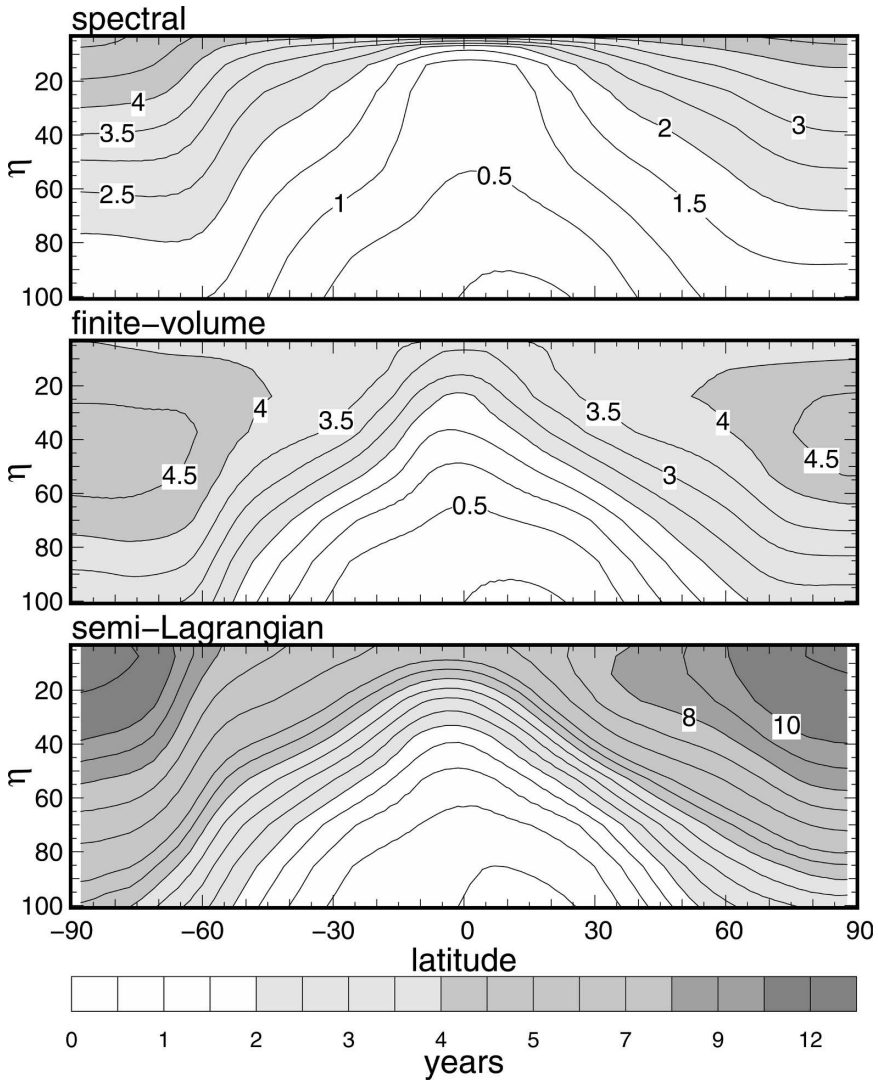

FIG. 7. Zonally 6-yr-averaged age of air: (top) spectral, (middle) finite volume, and (bottom) semi-Lagrangian.

and useful method is to calculate the lag time (Waugh and Hall 2002), defined to be the time required for a tracer at a given location to reach the same mixing ratio as that seen at the tropopause in the presence of a monotonic increase in the mixing ratio there. The lag time is believed to correspond to the mean age (the first moment of the age spectrum defining the mixing ratio) to within 10% for the stratosphere (Waugh and Hall 2002).

Figure 7 shows the lag time τ_{SF6} calculated from the zonal average of SF_6 for the three models. We have calculated τ_{SF6} for each of the last six years of the 10-yr simulation and averaged them. We show only the model regions above 100 hPa. It is important to note that all these model configurations are run with 26 vertical layers, having a model top layer located at between 2 and 4 hPa (35–40 km), and nine layers at or above 100 hPa. While age of air is frequently used as a diagnostic of model behavior in the middle atmosphere (Hall et al. 1999; Eluszkiewicz et al. 2000), the current model configurations are not designed to provide a high quality simulation of the stratosphere, and it is well known that the relatively low vertical resolution and the low altitude of the upper boundary condition (UBC) will result in a relatively poor representation of stratospheric dynamics (Boville and Cheng 1988; Rasch 1986). Nevertheless, it is of some interest to understand the interactions between the stratosphere and troposphere even in

this situation, because most GCMs use a similar resolution when not configured with a middle atmosphere focus.

The differences in the stratosphere between model configurations are associated with a complex combination of processes. There are differences in transport specific to a region (resulting from the numerical technique being used) and there are changes in the global general circulation (due both to the UBC effects discussed below and the differences in the general circulation of the troposphere) as well as differences in the age of air due to the formulation of the upper boundary condition for the tracer's transport equation. The influence of the UBC is complicated by the presence of a computational sponge layer in the model that is designed to enhance dissipative dynamical processes in the top few model layers. The sponge layer is applied differently in the FV core from the other two model configurations. In the spectral and SLD cores the sponge layer is produced by the addition of an extra (second-order Laplacian) diffusion term in the top few layers. In the FV core a lower order (more diffusive) numerical method is used in the top few model layers. It is typical for modelers to ignore or exclude the sponge layers from consideration when focusing on the atmospheric dynamics, but these layers do have on influence on tracer distributions over a larger domain, as seen in Fig. 7.

The tracer UBC is also important. The FV core allows no air or tracer mass flux across the top model interface. The other two model configurations use an outflow boundary condition for tracers calculated with respect to velocities defined at cell centers (in this case the velocity defined at the midpoint of the top model layer). Although the vertical velocity at the top model interface is zero (implying no flux), it is not necessarily zero at the layer midpoint. Therefore, when parcel trajectories are upward at cell centers the tracers are allowed to leave the model domain, when they are downward, the parcels are assumed to enter the model domain with the mixing ratio of the top model layer (Williamson and Rasch 1994). In the limit of vanishingly small top layer thickness, the tracer flux would go to zero also, although this is not the case for the current model configuration.

Although there are common features across models (e.g., longest ages in the polar regions, shortest in the Tropics), the three model configurations behave quite differently from each other. Vertical transport in the tropical stratosphere is very rapid in the spectral model, with τ lying below one year to pressures of 20 hPa. The semi-Lagrangian core has a very long lag time, with a value of 4 yr in the same region. The FV core lies in between the other two models with lag times of 2.5–3 yr.

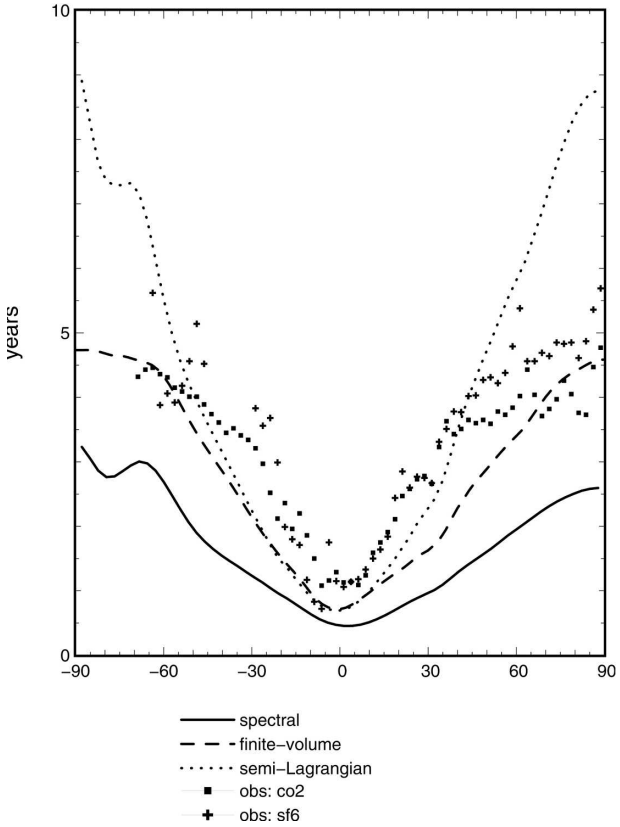

FIG. 8. Zonally 6-yr-averaged age of air at 20 km from SF_6. Observational estimates from CO_2 and SF_6 measurements.

The polar simulations are also very different, with ages near the model top between 5 and 15 yr for the spectral and SLD cores, respectively, and the FV model lying in between. The simulations are also very different near 100 hPa. The spectral simulation shows rapid air exchange between the troposphere and stratosphere, with age of air less than 2 yr at that pressure level, while the age of air in the other model configurations are 2 to 4 times that.

Figure 8 compares these age estimates interpolated to 20 km, and compared to the composite estimates produced by Waugh and Hall (2002) that were assembled from CO_2 observations of Boering et al. (1996) and Andrews et al. (2001), and SF_6 estimates of Elkins et al. (1996), Ray et al. (1999), and Harnisch et al. (1996). The age of air of the spectral model is clearly too young from pole to pole. Both SLD and FV models are much closer to the observed age between 60°N and 60°S. The observational estimate of about 5 yr in Northern Hemisphere polar regions compares more closely to the FV core estimates.

d. Neutral biosphere tracer

The changing concentrations of CO_2 arising from anthropogenic emissions (with its recognized importance as a greenhouse gas) have produced increasing attention on distributions of CO_2 and its sources and sinks over the last several decades. To characterize future CO_2 levels quantitatively, it is important to understand its sources and sinks. The observed distribution of CO_2 near the surface, along with chemical transport models, has been used as one mechanism for connecting a sink of anthropogenic CO_2 to the terrestrial biosphere (Pearman and Hyson 1980; Denning et al. 1996a,b; Randerson et al. 1997; Gurney et al. 2002). While CO_2 is a relatively well-mixed gas in the troposphere with variations of only a few percent spatially and temporally, the variations in its distribution at this level are quite sensitive to chemical and physical sources and sinks. To trust inferences about sinks of CO_2, we must be able to trust our ability to model the processes that control its distribution.

The observed meridional gradient in CO_2 is controlled by the locations of anthropogenic emissions (dominant in the Northern Hemisphere), the basic transport processes responsible for moving tracers from one region to the other, and correlations between transport processes and uptake and emission from the biosphere associated with the diurnal and seasonal changes in respiration and photosynthesis. The latter phenomena, frequently termed CO_2 rectification, arises because respiration (uptake of CO_2) tends to occur when the atmospheric boundary layer is most stable, at night and in winter, while photosynthesis (release of CO_2) occurs when the boundary layer is frequently unstable, during the day and in summer. The result (Denning et al. 1996a,b, and as seen below) is that a constituent that has a strong diurnal and seasonal cycle but a zero net flux in terms of the annual mean will produce a significant annual mean meridional gradient. There is both a seasonal rectification and a diurnal rectification effect.

Denning et al. (1995) showed that the meridional gradient of a CO_2-like constituent using purely seasonal fluxes and transport was approximately half as strong as that created by fossil fuel combustion sources, which led to a calculated net sink in the terrestrial biosphere that was stronger than would have been inferred otherwise. Denning et al. (1996b) showed that the effect of the diurnal variation of the biosphere had a very strong effect on annual mean CO_2 concentrations in the Tropics, but was less important in modulating the middle latitudes. Gurney et al. (2002) showed that neglecting the rectifier effect moved the inferred terrestrial sink of CO_2 south and west of the location retrieved from an inversion using sources with no seasonal cycle. That study also concluded that the rectification process is the major source of uncertainty in amplitude and location the Northern Hemisphere sink needed to explain the measured atmospheric CO_2 distribution.

In this study we have examined the sensitivity of the distribution of a CO_2-like tracer with a biosphere-like source/sink to the numerics of transport and dynamics, the presence or absence of a diurnal variation in emissions, and the relative phase of the diurnal variations of emissions and transport. Our motivation for the latter experiment is that there are well known deficiencies in the phase and amplitude of many modeled processes that affect both the sources and sinks of CO_2 and in the venting processes that allow exchange of air between the biosphere and the free troposphere. For example, Rasch et al. (2006) show that there are many regions where the diurnal phase of precipitation, which can be used as a proxy to indicate times of vigorous vertical transport of trace constituents, differs substantially between models and observations.

We use sources that have a zero net annual mean flux and that follow the patterns appropriate for biospheric photosynthesis and respiration (thus the name neutral biosphere tracer). Our base source/sink inventories come from the Carnegie–Ames–Stanford Approach (CASA) model (Potter et al. 1993) following the work of Randerson et al. (1997) and Olsen and Randerson (2004). This inventory has an estimated diurnal variation with data available every 3 h. We have also averaged the data to produce an equivalent inventory with exactly the same monthly mean average, and, as an exercise in understanding the importance in the relative phase of the diurnal cycle of emissions and the diurnal cycle of transport, have produced a shifted inventory where the source/sink occurs six hours later than the standard inventory. All figures show NB anomalies, defined as the NB mixing ratio after subtracting the initial mixing ratio.

Figure 9 shows the annually averaged surface concentrations for nine different model configurations. These configurations explore sensitivity to source type (separate panels in the figure), and dynamical core (common dynamical cores are flagged by line type). We first note that these solution span the range of the 17 different transport models explored in the TRANSCOM III model intercomparison of Gurney et al. (2003), even though that study used only monthly mean emissions. It is thus possible to get a very wide range of model behavior even in the context of a model with a common set of physical parameterizations. This suggests that some caution is needed in interpreting the TRANSCOM III model intercomparison, as it is certainly possible

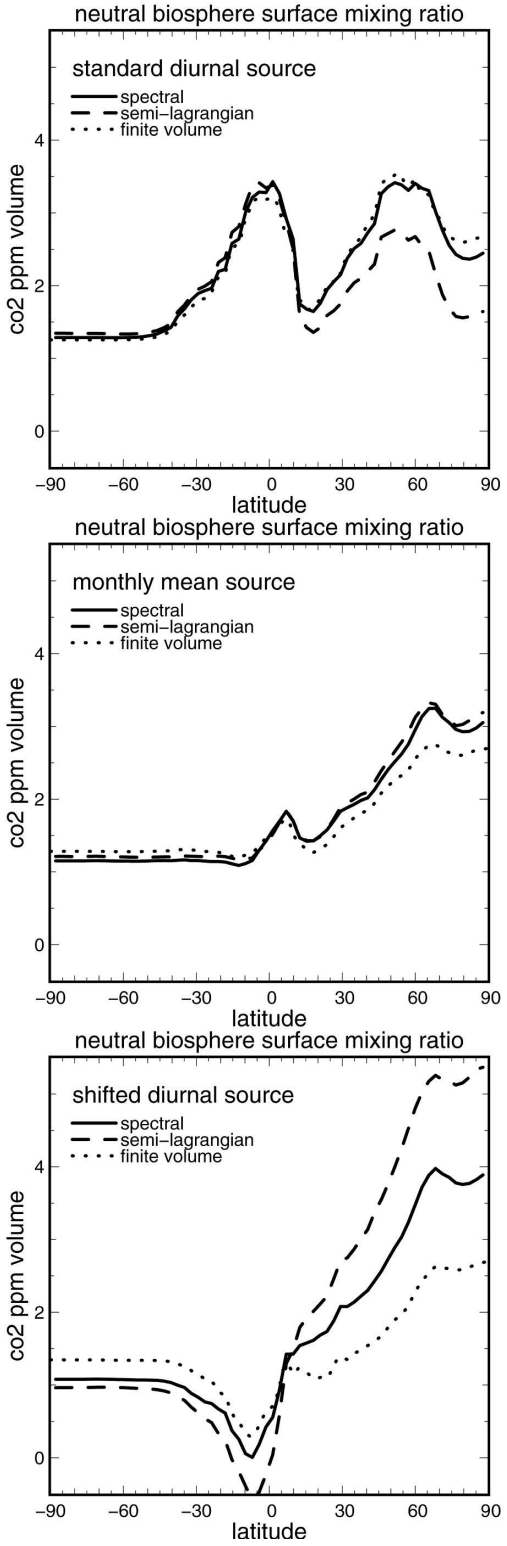

FIG. 9. Zonally averaged concentrations of the NB tracer anomaly at the surface for the nine cases discussed in the text. The anomaly is defined with respect to the initial concentration of the NB tracer: (top) standard diurnal source, (middle) monthly mean source, and (bottom) shifted diurnal source.

that the range of model results examined in that study did not span the range of uncertainty present in the atmosphere or present in models when a diurnal variation is present. The only model configurations that are relatively insensitive to dynamical core used a monthly mean source. Models including a diurnal variation span a much wider range of interhemispheric gradients, and since this effect is important in controlling the gradient of CO_2, it should be included in models attempting to represent these features accurately. The top two panels are consistent qualitatively with the results reported in Denning et al. (1996b), which showed that the seasonal cycle of the surface concentration of CO_2 (which can be interpreted as an offset from the background Southern Hemisphere value) was smaller at midlatitudes and larger in the Tropics in models including a diurnal variation in CO_2 uptake and emission compared to a model with only a monthly mean source, although quantitatively the difference in the tropical signature seems to be much larger than Denning saw.

The shifted diurnal source, on the other hand, enhances the interhemispheric gradients and reverses the sign of the deviation from the background value in the Tropics, indicating that the relative phase of emission and transport is a critical parameter in the interpretation of the CO_2 signal at the surface.

The distributions for the sources that include a diurnal variation are quite sensitive to the dynamical core. When the standard diurnal source (upper panel) is used, the SLD core is an outlier, with a significantly lower interhemispheric gradient than the other two model configurations. When the shifted diurnal source is used (lower panel), the SLD scheme has the highest interhemispheric gradient.

Figure 10 shows the vertical distribution of the NB tracer anomaly for the three different source distributions and its response to changes in the model core and to anthropogenic forcing, in a manner similar to Figs. 4 and 6. The lowermost panels show the effect of the sources. The simulations of annual-mean NB concentration are strongly modulated by atmospheric rectification. The depth of the anomaly associated with enhanced NB concentrations is strongly modulated by the phase difference of the diurnal variation of the source/sink. The anomaly is restricted to a narrow boundary layer with the standard diurnal source, and extends through a very deep region with the shifted diurnal source. The monthly mean source lies in between the two other simulations. The signal is reversed in the tropical regions with the anomaly propagating most deeply with the standard diurnal source. These panels also indicate the amplitude of the rectifier signal decreases with altitude, but it is clearly perceivable up to

tropopause levels, and even at these levels, the phasing of the rectification is important. The figures suggest that there will be a region, particularly in the upper northern hemisphere, where the rectification results in a substantial depletion of the NB tracer.

The uppermost panels of Fig. 9 indicate that the rectification is amplified at midlatitudes (by as much as 20%) in the FV core, and reduced at midlatitudes (by 40%–60%) in the SLD core. The tropical signatures for rectification are less sensitive to the numerics of the dynamics and transport algorithm than middle and high latitudes with differences of <20% between model versions. It is interesting to note that the signal of rectification extends more strongly into the lower stratosphere in both the SLD and FV cores compared to the spectral core in spite of the reduced STE in both model configurations compared to the spectral core. The middle panels of Fig. 9 remain consistent with the signals seen in radon and SF_6, with STE increasing as anthropogenic forcing increases.

e. Stratospheric sources of trace constituents

It is a common experience in global models [both GCM and chemical transport models (CTMs)] attempting a simulation of the photochemistry of the troposphere that midlatitude exchange of air between the stratosphere and troposphere is judged to be too vigorous, and this results in fluxes of ozone (O_3) that can exceed estimates based on observational evidence by as much as a factor of 4 (Crutzen et al. 1999; Bey et al. 2001; McLinden et al. 2000). This overestimate is believed to be due to a variety of factors, including errors in the numerical discretizations, the choice of computational vertical coordinate system that fluctuates substantially with respect to quasi-material surfaces in the atmosphere resulting in movement across model coordinate surfaces that are an artifact of the choice of model coordinate surfaces, and the use of meteorological fields arising from a data assimilation procedure that produces high frequency noise in the meteorology that act to mix ozone rapidly (Douglass et al. 2004).

The excessive downward ozone transport has important impacts on the simulation of many chemical species and on the climate of GCMs that include interactive chemistry, because ozone is both a very reactive gas and an important greenhouse gas. The biases introduced by the excessive transport are so large that special procedures have been designed to reduce the problem. One such method is the use of a synthetic source of stratospheric ozone, with a prescribed distribution and amplitude formulated to produce a precise amount of ozone in the global average. Since a fixed amount of ozone is produced as a source in the stratosphere, the model must produce a corresponding flux across the tropopause once the stratospheric burden equilibrates. Such a scheme was suggested by McLinden et al. (2000) who named the scheme SYNOZ and set the global integral to 475 Tg ozone per year. The result of using such a source is that the cross-tropopause transport, and troposphere ozone-mixing ratios correspond much more closely to observations than when mixing ratios of ozone are prescribed in stratosphere for models with large STE.

Ozone thus serves as a sensitive indicator of transport properties across the tropopause, and an important metric for models that require an accurate formulation for species important in the upper troposphere. For these reasons we have included two ozone-like test problems in the suite examined in this paper, a SYNOZ simulation following McLinden et al. (2000), and a tracer we call POZONE (standing for prescribed or pseudo ozone), in which we fix the ozone-mixing ratio to a uniform value at pressures less than 50 hPa. Both species are destroyed instantly at the surface. The tropospheric distribution of each specie is thus controlled by the flux from the stratosphere to the troposphere and the sink at the surface.

The two ozone-like species display the same problems characteristic of ozone using more realistic representations of ozone. Fig. 11 show simulations for the POZONE tracer. The lower panels show zonal, annual-averaged mixing ratios for cases with the three dynamical cores. The spectral and SLD cores are quite similar to each other. Both distributions have substantial intrusions of stratospheric air descending in the subtropics. Low mixing ratios are seen in the tropical region, indicative of air that has been depleted of ozone by recent contact with the surface layer. The figures themselves and the ratio of zonal averages seen in the two upper panels show that the SLD core has mixing ratios a factor of 2 to 4 times smaller in the Tropics than the spectral solution, and 2 to 3 times larger in the Southern Hemisphere polar troposphere. The difference in the equator to pole gradient between the two runs could be due to a more vigorous vertical mixing between the upper troposphere and surface, or to less vigorous mixing between the Tropics and subtropics, or to some combination of the two. The FV simulation differs substantially from the other two solutions. There is much less ozone throughout the troposphere than either of the other two simulations. The pole to equator ratio of ozone in the model is about the same as in the SLD solution, and a factor of 2 higher than the spectral solution. The signature of a much-reduced, cross-tropopause flux seen in these figures is also reflected in

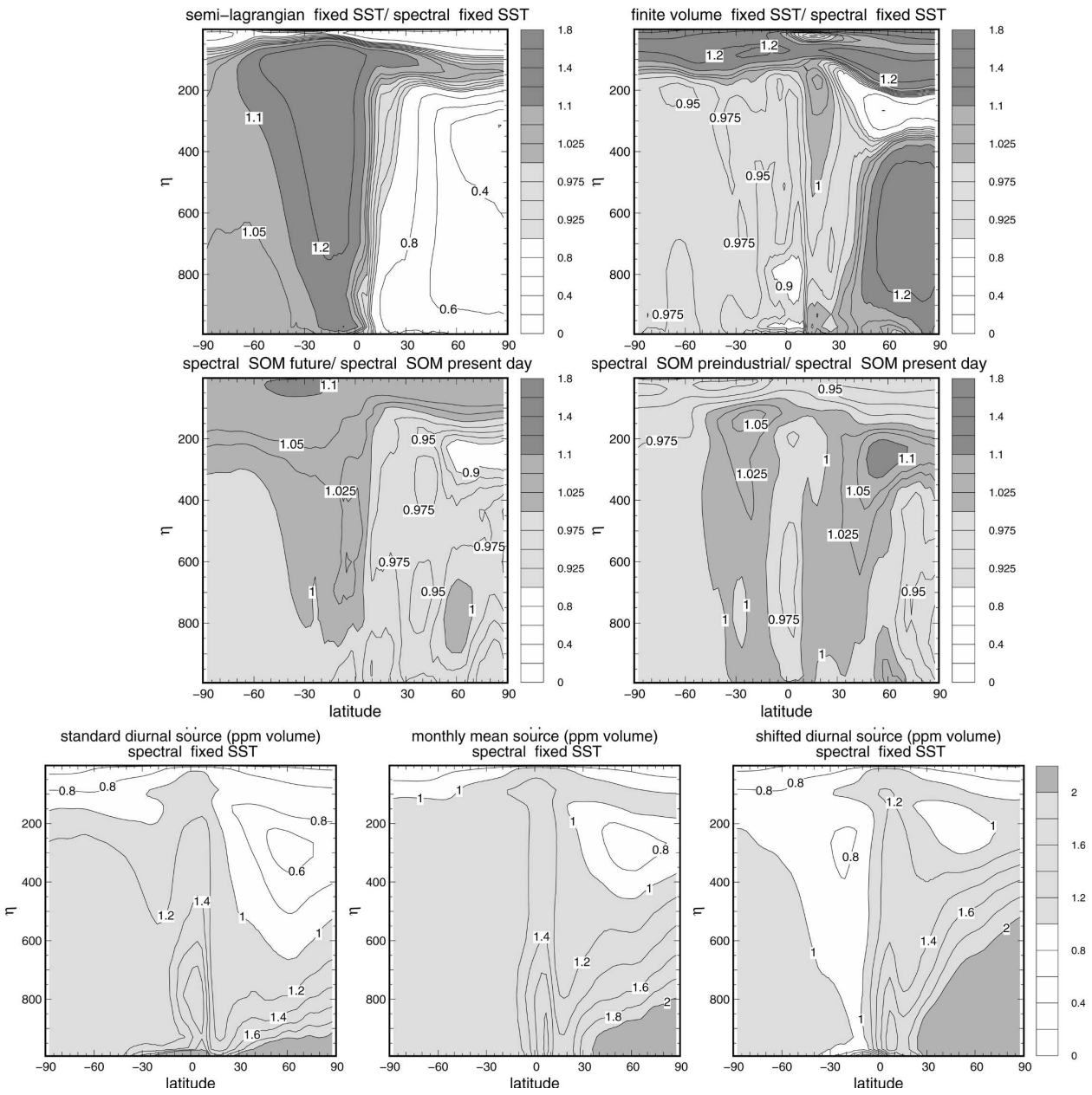

FIG. 10. Zonal averaged mixing ratio of NB tracers. (bottom) The spectral T42 simulations using the three different source inventories (standard diurnal, monthly mean, and shifted diurnal from left to right, respectively). (top four panels) Ratios of zonal annual averages for different cases compared to the spectral model with the standard diurnal source. The middle panels show the response of the spectral core to changes in anthropogenic forcing, and the upper panels show the response of the model to changes in the dynamical core.

the annually averaged ozone burden and cross-tropopause flux. The cross-tropopause flux of POZONE is a factor of 3 higher in the spectral core than the FV core.

The figures showing changes in transport circulation associated with anthropogenic forcing (middle panels of Fig. 11), suggest that the largest changes occur near the tropopause in the Southern Hemisphere pole, with decreases in POZONE in that region by 20%–30% as one moves from a preindustrial to present day to future climate regime, which can be explained by a corresponding increase in STE in the lowermost polar stratosphere. This feature again is consistent with the conclusions of Rind et al. (2001) who found enhanced STE in

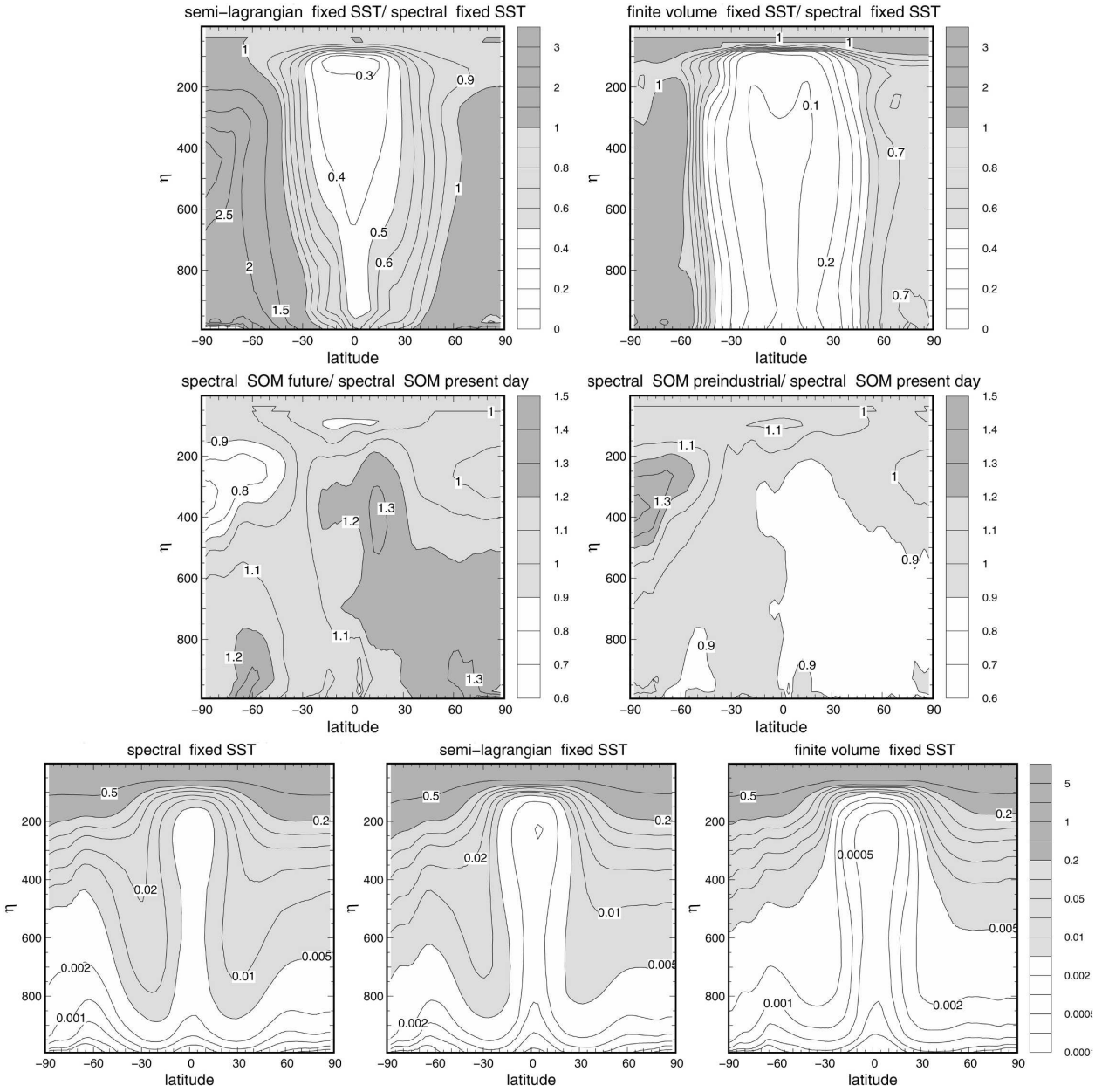

FIG. 11. (bottom) Zonal averaged mixing ratio of pseudo ozone for the base cases for the three dynamical cores and (top four panels) ratio of various cases to spectral dynamics base case. Note that the contour intervals for the lower panels are distributed approximately logarithmically, with values of 1, 2, and 5×10^n, where n is an integer.

this region and an enhanced leakiness of the tropical pipe in the stratosphere.

Figure 12 shows simulations for the SYNOZ tracer, for the spectral and FV models (an SLD simulation was not made), with a focus on the upper troposphere and stratosphere. There is less difference between these two models for SYNOZ than for the POZONE tracer. Although the global signatures of the previous species indicate that the STE in the FV core is lower overall than the other model cores, the lower panels indicate that the mixing ratios at the South Pole tropopause region are actually higher (by about a factor of 2) than the spectral model, although this feature is restricted to a relatively small geographic region.

The upper panels display ratios between POZONE and SYNOZ for a particular dynamical core. The figures suggest that the cross-tropopause transport processes are acting very differently in the spectral and FV

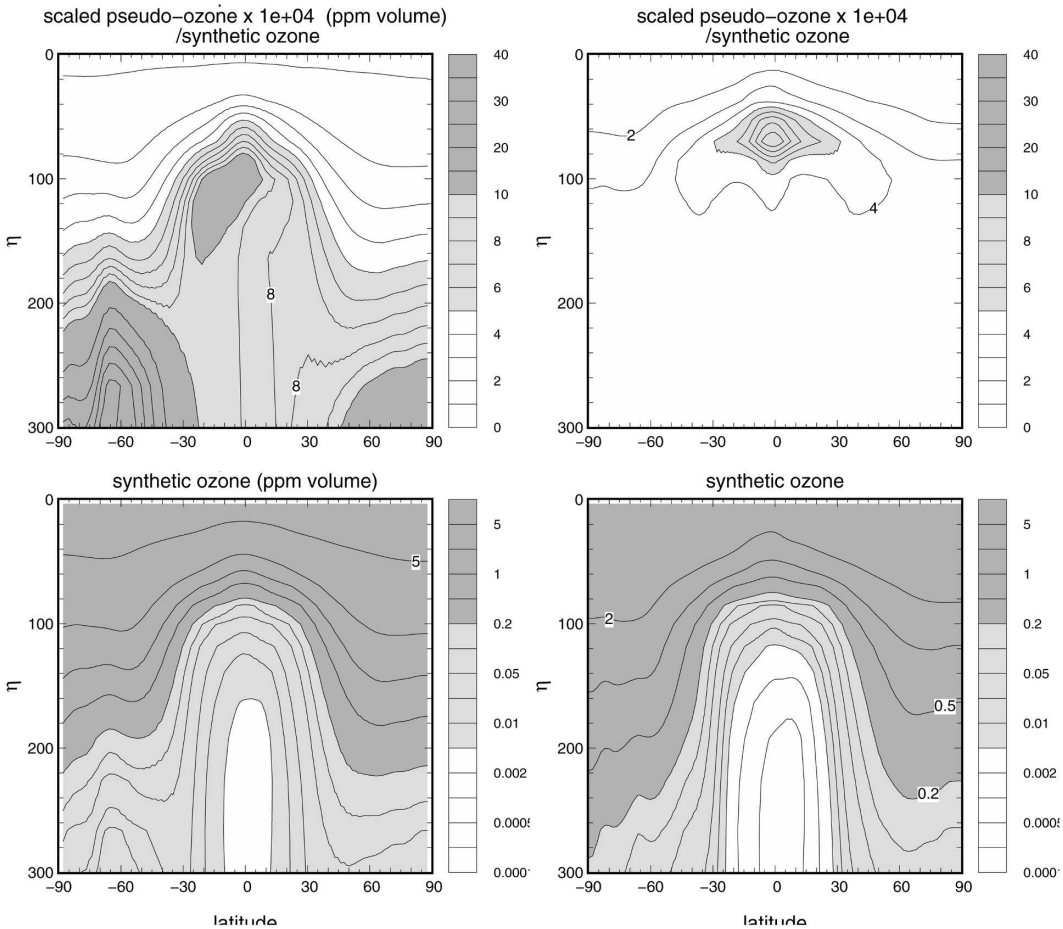

FIG. 12. (bottom left) Zonal averaged mixing ratio of SYNOZ for the spectral T42 and (bottom right) the FV runs. (top) Ratio of POZONE to SYNOZ: (left) spectral model and (right) FV model.

core. In the FV core, the ratio of the two tracers is almost uniform, with a value near three over the whole troposphere and the lowermost stratosphere. The one region that has a significant departure from this value is in the Tropics, above the tropical tropopause between 60 and 80 hPa where the ratio reaches a value of nine, a factor of 3 enhancement over any other region in the model atmosphere. This suggests that there is a path for preferred transport of POZONE-rich air to this region that is not present for SYNOZ air. Recall that the POZONE source is located between 0 and 50 hPa and the SYNOZ source is located between 10 and 80 hPa. If the mixing ratios in the region from 60 to 80 hPa were entirely controlled by the proximity to the source, then the ratio of POZONE/SYNOZ would be lower here than in any other region, rather than higher, as seen in Fig. 12. In order for the ratio to reach a maximum, POZONE-rich air from elsewhere must be mixed rapidly into this region, and SYNOZ-source air must be exported rapidly from this region.

This picture contrasts with that seen in the spectral dynamical core (upper left panel of Fig. 12). In this dynamical framework, ratios vary between 3 and 30 over a very large spatial region of the upper troposphere. The explanation for this difference is that there must be very rapid exchange of air between stratosphere and troposphere from regions where the POZONE source is important (e.g., midlatitudes), and a much less rapid exchange in regions where the SYNOZ source is important. Also, the exchange occurring within the stratosphere between the SYNOZ and POZONE region is taking place much more slowly than the exchange between POZONE and the troposphere. To summarize, this rather complex interpretation is consistent with a picture of the model STE in which much more exchange is occurring in the spectral core between midlatitudes and the troposphere than is occurring in the FV core.

In addition to changes in the mean distribution of tracers, changing dynamical cores and advection

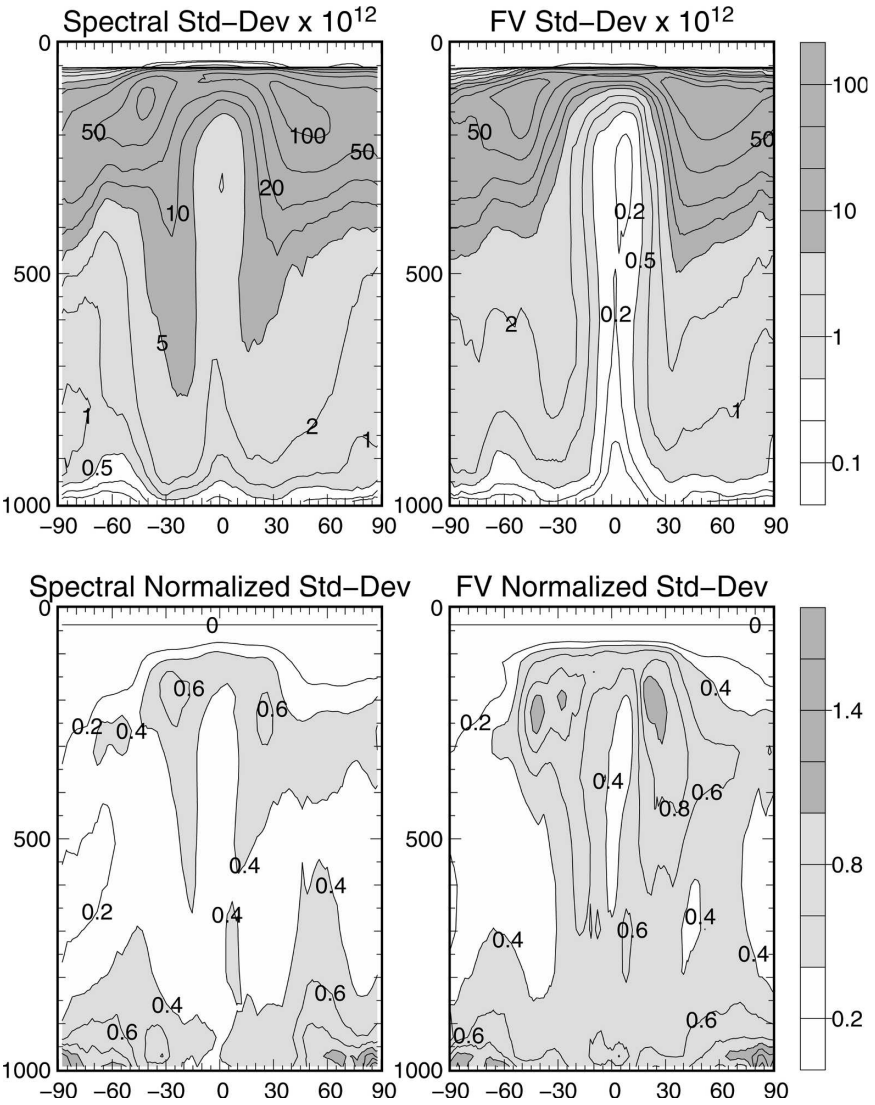

FIG. 13. Variability of the POZONE tracer about monthly means for the model. (top) The regular standard deviation. (bottom) The standard deviation of POZONE normalized by the monthly mean value. Left panels show results for the spectral core, right panels show results for the FV core.

schemes and/or changing climates may change the variability of the distributions. We have examined two types of model variability: within-monthly variability and between-monthly variability. We define within-monthly variability to be the standard deviation of daily data about the monthly mean, and the between-month variability to be the standard deviation of a given month of the year about the ensemble mean for that month.

We have found the within-monthly variability to be larger than the between-monthly variability for all the tracers considered here (not shown). For most of the tracers studied, the variability also does not change when a different advection scheme/dynamical core is used, with the exception of the POZONE tracer for the within-monthly variability, where differences in the variability are seen between the FV and the spectral (or semi-Lagrangian) core throughout much of the troposphere (Fig. 13). We show the standard deviation in the upper panels, and the standard deviation normalized by the annual average value in the lower panel. Both the annual mean ozone and the standard deviation are lower in the FV case, but the within-monthly variability (standard deviation/mean) is higher.

f. Tracer/dynamics consistency

D. Johnson (University of Wisconsin, personal communication) has proposed an interesting variant on evaluation procedures introduced in previous work by him and his colleagues (Johnson et al. 2000, 2002). The earlier procedures were used to evaluate the behavior of conserved tracers in the presence of numerical errors. Those studies used equivalent potential temperature as a tracer, and thus were quite sensitive to the formulation for water vapor evolution as well as to formulation for the model thermodynamics. The new procedure provides a simultaneous test of the ability of the model to transport conserved tracers consistently and the ability of the model to maintain a specific nonlinear relationship between six different conserved and nonconserved variables that are influenced by adiabatic and nonadiabatic processes and by subgrid-scale and resolved-scale dynamical processes. The procedure follows from a particular expression for the first and second law of thermodynamics. The expression, derived in the appendix, can be written as

$$\theta_1 = \left(\frac{\theta_0}{T_0}\right) T_1 \left(\frac{p_0}{p_1}\right)^{R/C_p p}. \quad (1)$$

Here the subscripts 0 and 1 indicate values of the variables at two points separated in space and time. Here, θ is a variable proportional to the exponent of the entropy; T and p are the temperature and pressure, and R and C_p the gas constant and specific heat at constant pressure appropriate for dry air.

Equation (1) can be used to define the potential temperature by assigning the value of θ_0 to be T_0, p_0 to be 10^5 Pa, and to drop the subscript from (θ_1, T_1, p_1), but we observe that Eq. (1) defines a more general relationship between this set of variables at any two points in space and time connected by a trajectory, even in the presence of entropy (potential temperature) sources and sinks, since T_1, p_1, and θ_1 should evolve in a consistent fashion even in the presence of those sources and sinks. The test that Johnson proposed goes as follows:

- Consider (θ_0, T_0, ${p_0}^{R/C_p}$) as passive tracers, advected with the flow. Set the initial conditions for these tracers to be the conventional potential temperature θ, temperature T, and pressure p at the initial time. Choose p_1 and T_1 to be the value of T and p at a location in space and time and use Eq. (1) to predict θ_1 at that grid point.
- Compare θ_1 to the conventional θ calculated from T and p. If they agree closely, then the model is simultaneously reproducing the first law of thermodynamics, providing an accurate numerical representation of the other equations of motion, and maintaining an accurate relationship between variables as they evolve.

We note that this is quite a difficult feat. This test requires accurate representations of individual constituents in the presence of spatially and temporally varying sources and sinks of heat. Furthermore, the numerical equations are not formulated in a manner designed explicitly to satisfy Eq. (1). The difference between θ_1 and θ identifies inconsistencies in the model. The inconsistencies arise for the following reasons:

- There are errors in the advection operators that will result in the θ_0, T_0, and ${p_0}^{R/C_p}$ not being advected accurately as passive scalars.
- The numerical implementation of the advection operators are nonlinear, and the nonlinear combinations of these nonlinear operators need not satisfy any a priori external relationships like Eq. (1).
- There are errors in all other discretizations of the thermodynamic, mass continuity, and hydrostatic equations, which will introduce errors in the evolution of the temperature and pressure.
- There are inconsistencies introduced in each solution of Eq. (1) within the dynamical core because of the choice of thermodynamic and dynamic variables. For example, the spectral and SLD formulations use T as the predicted thermodynamic variable and ln P_S (the surface pressure) as the predicted mass variable for the model, while the FV model uses θ_v (the virtual potential temperature, which is a valid choice in the absence of sources or sinks of water vapor), and δp the mass of air in a layer as the predicted mass variable.

Figure 14 shows scatter diagrams of θ_1 versus θ after ten days of simulation in the three dynamical cores. Although the model domain extends to 35 km (corresponding to potential temperatures as high as 1200 K) we have chosen to display a range of values appropriate to the surface through the lower stratosphere (20 km), so the range displayed is restricted to potential temperatures between 200 and 500 K. Table 2 shows the root mean squared (rms) error of ($\theta - \theta_1$) for the whole model domain for each model, including the part of the domain excluded from the figure. The largest errors are seen in the spectral simulation, with rms errors about a factor of 2 higher than seen in the other two model configurations. The spectral simulation shows large errors occurring at temperatures in the range of ~400–500 K, corresponding to values in the upper troposphere and lower stratosphere (UTLS) ranges. The diagnosed θ_1 is systematically lower than θ. This result is

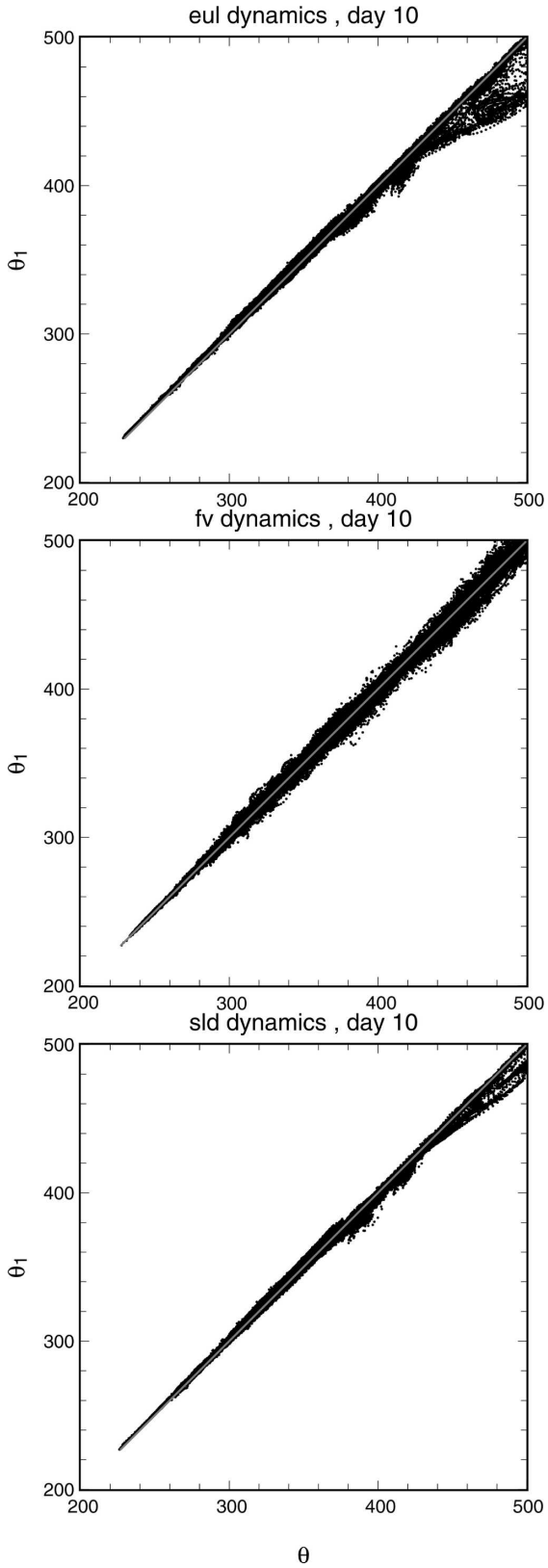

FIG. 14. Variable θ vs θ_1 at day 10: (top) spectral (eul), (middle) FV, and (bottom) SLD dynamics.

TABLE 2. Rms errors on day 10 for the potential temperature as calculated from Eq. (1) and calculated using the conventional equation. Right-hand-side column indicates the rms error when weighted by the air mass in the cell normalized by the global air mass.

Case	Rms error (K)	Weighted rms error (K)
Spectral	9.09	5.48
Finite volume	4.1	2.67
SLD	4.6	3.13

consistent with the earlier work of Johnson et al. (2000, 2002), who showed a similar result for their earlier tests of CCM2 and CCM3 using either reversible dry or moist adiabatic thermodynamics, although the discrepancies in this study are substantially lower than those seen in their tests. This may be due to the improvements in model energetics, which required significant modifications to the physical parameterizations (Boville and Bretherton 2003; Boville et al. 2006), or the differences associated with the use of θ (this study) versus θ_e in the Johnson studies. Johnson et al. (2000) and Johnson et al. (2002) showed very large errors in CCM simulation near the surface at temperatures ranging from 290–320 K, which were attributed to the formulation of the interpolation scheme chosen in the semi-Lagrangian transport algorithm. Our simulations do not show these errors, presumably because our test involves a conservative variable that does not include water vapor, while the studies by Johnson et al. used θ_e, which does. Johnson et al. explained the large errors they found as a consequence of the lack of continuity of derivatives of the interpolating polynomials used in the formulation, and the method utilized for calculating the interpolating polynomials near boundaries. The errors were substantially reduced when they changed the form of the interpolating polynomial.

The simulations using the spectral and SLD cores (upper and lower panels, respectively), show a systematic bias, with θ_1 frequently lower by 10–20 K compared to the value of θ calculated from T and p. This result is very similar to the studies by Johnson et al. (2000, 2002), who explained this bias in terms of the problems with continuity of the interpolating polynomials. The fact that the SLD core biases are smaller than those of the spectral core may be explained by the fact that the same interpolating polynomial forms are used for all fields in the SLD core, and that in the spectral core, different formulations are used for the model thermodynamics, the model moist variables, and passive tracers θ_0, T_0, and p^{R/C_p}. The inconsistent discretization may be manifested by large errors in θ_1 compared to θ.

There is no bias in the θ_1 estimate of θ in the FV core, indicating that the internal consistency of the formulation is higher than the other two model cores.

4. Summary and conclusions

This study has examined the sensitivity of a number of important archetypical tracer problems to the numerical method used to solve the equations of tracer transport and atmospheric dynamics. The tracers' scenarios were constructed to exercise the model for a variety of problems relevant to understanding and modeling the physical, dynamical, and chemical aspects of the climate system.

We have examined a few short (<30 days) simulations and shown that the models do behave very differently for these short-lived species. The largest signal was seen near the tropopause, where the FV core shows a much reduced level of vertical and meridional mixing. There was also evidence that the subtropical subsidence regions are more isolated from Tropics and midlatitudes in the FV core than as seen in the other model simulations.

Simulations of radon were used to explore differences between the models for a short-lived tracer emitted from the surface that is more strongly influenced by rapid, subgrid-scale transport. The simulations were quite similar between the surface and 400 hPa, equatorward of about 60°, with mean concentrations differing at the 5% level in this region. The simulation differed more strongly in the upper troposphere, where both the FV and SLD cores showed 10%–20% higher concentrations and much lower concentrations in the stratosphere. We interpret this result to be a consequence of reduced stratosphere/troposphere exchange in these two model configurations compared to the spectral core. The FV core showed substantially (20%) higher concentrations in the northern polar regions indicating more meridional mixing between midlatitudes and Tropics than the other cores. Manifestations of substantial differences between the polar tropopause temperature distribution in the SLD core compared to the other cores were easily discernible in the radon distribution, indicating that the polar temperature bias present in all versions of the CAM and in most other GCMs has an influence on tracer distributions and one should anticipate that improvements to this aspect of the GCMs will result in changes in trace specie distributions as well.

We used SF_6 as a measure of interhemispheric transport and exchange between troposphere and stratosphere (age of air). The results for STE processes are consistent with the radon study in that the spectral core showed much higher STE than either of the other cores. A comparison with estimated age of air from CO_2 and SF_6 measurements in the stratosphere suggest that the FV core is behaving most realistically.

We used a neutral biosphere test case to explore issues of diurnal and seasonal rectification of a tracer with sources and sinks at the surface. The sources and sinks have a zero annual average, and the rectification is associated with temporal correlations between the sources, sinks, and transport. We also examined the sensitivity of the result to shifts in the correlations between transport and source/sink terms. While Denning et al. (1999) concluded that subgrid-scale, parameterized version transport provided the most obvious explanation for differences between models for long-lived species, and that model development should focus on improvements to this aspect of the tracer transport rather than on improved numerical schemes for horizontal advection, our study suggests that although this conclusion is valid, the model sensitivity is more subtle than might be apparent at first. We have used a model in which the subgrid-scale parameterizations themselves are nearly identical. The only differences were due to small changes in tuning between the FV core and the other two cores (spectral and SLD). The test suggests that the rectification is strongly influenced by the resolved-scale dynamics (i.e., the dynamical core) and that the numerical formulation for dynamics and transport still plays a critical role in the distribution of NB-like species. Since the distribution of species driven by these processes have a strong influence on the interpretation of the missing sink for CO_2, and our interpretation of climate change associated with anthropogenic forcing, these issues should not be neglected.

Two test cases were used to explore exchange between the stratosphere and troposphere. Both tracers had a source in the stratosphere and a sink at the surface. We used a pseudo-ozone (POZONE) tracer with an unlimited source, designed to replenish ozone to a prescribed value above 50 hPa, and a synthetic-ozone (SYNOZ) tracer with a prescribed production rate in the tropical stratosphere to explore the role of STE in a model configuration similar to that used by many global atmospheric models of tropospheric photochemistry. The two tracers provide information about the rate at which air is exchanged between the Tropics and extratropics in the stratosphere, and the rate at which air is exchanged between the stratosphere and troposphere. The POZONE tests showed that the spectral and SLD core configuration had much more rapid downward transport at midlatitudes than the FV core (much shorter exchange time between stratosphere and troposphere). The ratio of SYNOZ to POZONE showed

that the exchange time between Tropics and midlatitudes in the stratosphere was much slower than the exchange time between stratosphere and troposphere in the spectral core, while in the FV core the exchange times were much closer to each other.

We examined changes in variability (defined as the standard deviation over the mean) due to dynamical core changes and climate. Small changes in variability were seen between climates, while discernible changes in the variability between the finite volume dynamical core and the other two cores were seen in the ozone tracer simulation.

We also explored the ability of each model core to simultaneously transport an array of trace constituents obeying a complex nonlinear relationship and having complex sources and sinks. The nonlinear relationship is dictated by the first and second law of thermodynamics, and the test provided a rigorous means of exploring the model's abilities to satisfy these equations and the equations describing mass conservation. The spectral core showed the largest departures from the predicted nonlinear relationship. The FV and SLD models both produced errors a factor of 2 lower. The SLD model did show a small but systematic bias in its ability to maintain this relationship that was not present in the FV simulation.

The results of the study indicate that for virtually all of these problems the model numerics still has a large role in influencing the model solutions. It was frequently the case that the differences in solutions resulting from varying the numerics still exceeds the differences in the simulations resulting from a significant physical perturbation (like changes in greenhouse gas forcing). The simulations that explore the model response to changing climate associated with anthropogenic forcing indicate an increase in STE, consistent with previous studies by Butchart and Sciafe (2001), Rind et al. (2001), Collins et al. (2003), and Zeng and Pyle (2003), all of whom found an increase in mass exchange across the tropopause associated with more vigorous planetary wave forcing in the extratropics.

It is interesting to note that the changes in mass transport of tracers associated with climate change are swamped by the amplitude of changes associated with the numerical method used to formulate the model in virtually all the problems we explored. The perturbations associated with climate change may be robust, even if the mean state of a field (about which the perturbations exist) is sensitive to the numerics. This does not mean that the physical response of the system is not correct. Indeed, the fact that our results are consistent with the result from four other studies using three completely different numerical formulations for dynamics and transport lend some confidence to the conclusions of those papers, but this also indicates that all of the studies (including ours) are being affected by the numerical formulation, and caution is required in interpreting the results.

There are clear winners and losers in this intercomparison from the point of view of tracer transport. The FV core is conservative (neither of the others are), less diffusive (maintains strong gradients better), and the form of the thermodynamic equation maintains the nonlinear relationships among variables required by thermodynamic and mass conservation constraints more accurately. These criteria are among the reasons we anticipate moving to this core or some other with similar desirable properties as the standard configuration for future generations of CAM.

Acknowledgments. This work was supported in part by grants from the NASA Atmospheric Chemistry Modeling and Analysis Program (CMAP). We benefited from conversations with Scott Denning, Louisa Emmons, Don Johnson, Jean-Francois Lamarque, Jim Randerson, and Darryn Waugh. We thank the Don Johnson and an anonymous reviewer for their comments, and Christina Book for editorial assistance.

APPENDIX

Derivation of the Thermodynamic Forms Used in the Tracer Tests

We recall a form of the first law of thermodynamics (following Dutton 1976)

$$ds = C_v d\ln T + Rd\ln\alpha = C_p \ln T - Rd\ln p, \quad \text{(A1)}$$

where C_v and C_p are the specific heat at constant volume and pressure of a parcel, T and P the temperature and pressure of the parcel, s the specific entropy, and R the gas constant for the parcel. The second expression on the right is valid only for an ideal gas. This equation expresses the relationship between s, T, and (α or p). The integral form of the equation is

$$s_1 - s_0 = C_v \ln\frac{T_1}{T_0} + R\ln\frac{\alpha_1}{\alpha_0} = C_p \ln\frac{T_1}{T_0} - R\ln\frac{p_1}{p_0}. \quad \text{(A2)}$$

It is typical to define a function θ such that

$$s_1 - s_0 = C_p \ln\frac{\theta_1}{\theta_0} \quad \text{(A3)}$$

to give

$$\theta_1 = \left(\frac{\theta_0}{T_0}\right) T_1 \left(\frac{p_0}{p_1}\right)^{R/Cp}. \quad \text{(A4)}$$

In CAM, the first law is solved by writing Eq. (A2) in time-differentiated form as

$$\frac{ds}{dt} = \frac{C_p}{T}\frac{dT}{dt} - \frac{R}{p}\frac{dp}{dt} = Q/T, \tag{A5}$$

where we have introduced the alternate notation using $Q/T = ds/dt$ as a heating rate associated with dissipation, radiation, or phase change. The model solves the equation in an operator split form. That is, variables are updated sequentially for each physical process operating on the model. During the dynamics update in the spectral and SLD cores (A5) takes on the form

$$\frac{dT}{dt} - \frac{RT}{C_p p}\frac{dp}{dt} = 0, \tag{A6}$$

while the FV core uses

$$\frac{d\theta_v}{dt} = 0. \tag{A7}$$

Here θ_v is the virtual potential temperature, which is also a conserved variable in the absence of sources or sinks of water.

REFERENCES

Andrews, A. E., and Coauthors, 2001: Mean ages of stratospheric air derived from in situ observations of CO_2, CH_4, and N_2O. *J. Geophys. Res.,* **106,** 32 295–32 314.

Babiker, M., J. Reilly, M. Mayer, R. Eckaus, I. S. Wing, and R. Hyman, 2001: The MIT Emissions Prediction and Policy Analysis (EPPA) model: Revisions, sensitivities, and comparison of results. MIT Joint Program on the Policy and Science of Global Change Tech. Rep. 71, Massachusetts Institute of Technology, Cambridge, MA, 90 pp.

Bey, I., and Coauthors, 2001: Global modeling of tropospheric chemistry with assimilated meteorology: Model description and evaluation. *J. Geophys. Res.,* **106,** 23 073–23 096.

Boering, K. A., S. C. Wofsy, B. C. Daube, H. R. Schneider, M. Loewenstein, J. R. Podolske, and T. J. Conway, 1996: Stratospheric transport rates and mean age distribution derived from observations of atmospheric CO_2 and N_2O. *Science,* **274,** 1340–1343.

Boville, B. A., and X. Cheng, 1988: Upper boundary effects in a general circulation model. *J. Atmos. Sci.,* **45,** 2592–2606.

——, and C. S. Bretherton, 2003: Heating and kinetic energy dissipation in the NCAR Community Atmosphere Model. *J. Climate,* **16,** 3877–3887.

——, D. Jacob, and M. Prather, 1997: Global tracer transport models, proceedings of a WCRP workshop on the parameterization of subgrid-scale tracer transport. Tech. Doc., WMO/TD 823 26, World Meteorological Organization, 100 pp.

——, P. J. Rasch, J. J. Hack, and J. R. McCaa, 2006: Representation of clouds and precipitation processes in the Community Atmosphere Model version 3 (CAM3). *J. Climate,* **19,** 2184–2198.

Butchart, N., and A. A. Sciafe, 2001: Removal of chlorofluorocarbons by increased mass exchange between the stratosphere and troposphere in a changing climate. *Nature,* **410,** 799–802.

Collins, W. D., and Coauthors, 2004: Description of the NCAR Community Atmosphere Model: CAM3.0. Tech. Rep. NCAR/TN-464+STR, National Center for Atmospheric Research, Boulder, CO, 226 pp. [Available online at http://www.ccsm.ucar.edu/models/atm-cam.]

——, and Coauthors, 2006a: The Community Climate System Model, version 3 (CCSM3). *J. Climate,* **19,** 2122–2143.

——, and Coauthors, 2006b: The formulation and atmospheric simulation of the Community Atmosphere Model version 3: CAM3. *J. Climate,* **19,** 2140–2157.

Collins, W. J., R. G. Derwent, B. Garnier, C. E. Johnson, M. G. Sanderson, and S. S. Stevenson, 2003: Effect of stratosphere-troposphere exchange on the future tropospheric ozone trend. *J. Geophys. Res.,* **108,** 8528, doi:10.1029/2002JD002617.

Crutzen, P. J., M. G. Lawrence, and U. Poschl, 1999: On the background photochemistry of tropospheric ozone. *Tellus,* **51A,** 123–146.

Denning, A., I. Y. Fung, and D. Randall, 1995: Latitudinal gradient of atmospheric CO_2 due to seasonal exchange with land biota. *Nature,* **376,** 240–243.

——, G. Collatz, C. Zhang, D. Randall, J. A. Berry, P. J. Sellers, G. A. Colello, and D. A. Daazlich, 1996a: Simulations of terrestrial carbon metabolism and atmospheric CO2 in a general circulation model. Part 1: Surface carbon fluxes. *Tellus,* **48B,** 521–542.

——, D. Randall, G. Collatz, and P. Sellers, 1996b: Simulations of terrestrial carbon metabolism and atmospheric CO2 in a general circulation model. Part 2: Spatial and temporal variations of atmospheric CO2. *Tellus,* **48B,** 543–567.

——, and Coauthors, 1999: Three-dimensional transport and concentration of SF_6. A model intercomparison study (TransCom 2). *Tellus,* **51B,** 266–297.

Douglass, A. R., R. S. Stolarski, S. E. Strahan, and P. S. Connell, 2004: Radicals and reservoirs in the GMI chemistry and transport model: Comparison to measurements. *J. Geophys. Res.,* **109,** D16302, doi:10.1029/2004JD004632.

Dutton, J. A., 1976: *The Ceaseless Wind.* McGraw Hill, 579 pp.

Elkins, J. W., and Coauthors, 1996: Airborne gas chromatograph for in situ measurement of long-lived species in the upper troposphere and lower stratosphere. *Geophys. Res. Lett.,* **23,** 347–350.

Eluszkiewicz, J., R. S. Hemler, J. D. Mahlman, L. Bruhwiler, and L. L. Takacs, 2000: Sensitivity of age-of-air calculations to the choice of advection scheme. *J. Atmos. Sci.,* **57,** 3185–3201.

Feichter, J., and P. J. Crutzen, 1990: Parameterization of vertical tracer transport due to deep cumulus convection in a global transport model and its evaluation with ^{222}Radon measurements. *Tellus,* **42B,** 100–117.

Genthon, C., and A. Armengaud, 1995: Radon 222 as a comparative tracer of transport and mixing in two general circulation models the atmosphere. *J. Geophys. Res.,* **100,** 2849–2866.

Gurney, K. R., and Coauthors, 2002: Towards robust regional estimates of CO_2 sources and sinks using atmospheric transport models. *Nature,* **415,** 626–630.

——, and Coauthors, 2003: TransCom 3 CO_2 inversion intercomparison: 1. Annual mean control results and sensitivity to transport and prior flux information. *Tellus,* **55B,** 555–579.

Hall, T. M., and R. A. Plumb, 1994: Age as a diagnostic of stratospheric transport. *J. Geophys. Res.,* **99,** 1059–1070.

——, K. Boering, and R. A. Plumb, 1999: Evaluation of transport in stratospheric models. *J. Geophys. Res.,* **104,** 18 815–18 839.

Harnisch, J. R., R. Borchers, P. Fabian, and M. Maiss, 1996: Tropospheric trends for CF_4 and C_2F_6 since 1982 derived from

SF_6 dated stratospheric air. *Geophys. Res. Lett.,* **23,** 1099–1102.

Jacob, D. J., and M. J. Prather, 1990: Radon-222 as a test of convective transport in a general circulation model. *Tellus,* **42B,** 118–134.

——, and Coauthors, 1997: Intercomparison of convective and synoptic transport in global models using ^{222}Rn and other tracers. *J. Geophys. Res.,* **102,** 5953–5970.

Johnson, D. R., A. J. Lenzen, T. H. Zapotocny, and T. K. Schaack, 2000: Numerical uncertainties in simulation of reversible isentropic processes and entropy conservation. *J. Climate,* **13,** 3860–3884.

——, ——, ——, and ——, 2002: Numerical uncertainties in simulation of reversible isentropic processes and entropy conservation: Part II. *J. Climate,* **15,** 1777–1804.

Kiehl, J. T., C. Shields, J. J. Hack, and W. D. Collins, 2006: The climate sensitivity of the Community Climate System Model version 3 (CCSM3). *J. Climate,* **19,** 2584–2596.

Lin, S.-J., 2004: A "vertically Lagrangian" finite-volume dynamical core for global atmospheric models. *Mon. Wea. Rev.,* **132,** 2293–2307.

Liu, S., J. McAfee, and R. Cicerone, 1984: Radon222 and tropospheric vertical transport. *J. Geophys. Res.,* **89,** 7291–7297.

McLinden, C. A., S. C. Olsen, B. Hannegan, O. Wild, and M. J. Prather, 2000: Stratospheric ozone in 3-d models: A simple chemistry and the cross-tropopause flux. *J. Geophys. Res.,* **105,** 14 653–14 665.

Olsen, S., and J. T. Randerson, 2004: Differences between surface and column atmospheric CO2 and implications for carbon cycle research. *J. Geophys. Res.,* **109,** D02301, doi:10.1029/2003JD003968.

Otto-Bliesner, B. L., R. A. Tomas, E. C. Brady, C. M. Ammann, and Z. Kothavala, 2006: Climate sensitivity of moderate- and low-resolution versions of CCSM3 to preindustrial forcings. *J. Climate,* **19,** 2567–2583.

Pearman, G. I., and P. Hyson, 1980: Activities of the global biosphere as reflected in atmospheric CO_2 records. *J. Geophys. Res.,* **85,** 4468–4474.

Potter, C. S., J. T. Randerson, C. B. Field, P. A. Matson, P. M. Vitousek, H. A. Mooney, and S. A. Klooster, 1993: Terrestrial ecosystem production: A process model based on global satellite and surface data. *Global Biogeochem. Cycles,* **8,** 811–841.

Prather, M. J., and E. E. Remsberg, 1992: The atmospheric effects of stratospheric aircraft: Report of the 1992 models and measurements workshop. NASA Tech. Rep. 1292, 3 vols., 764 pp.

Pyle, J., and M. Prather, 1996: Global tracer transport models, report of a scientific symposium, Bermuda, 1990. WMO Tech. Doc. 24, World Meteorological Organization, 186 pp.

Randerson, J. T., M. V. Thompson, T. J. Conway, I. Y. Fung, and C. B. Field, 1997: The contribution of terrestrial sources and sinks to trends in the seasonal cycle of atmospheric carbon dioxide. *Global Biogeochem. Cycles,* **11,** 535–560.

Rasch, P. J., 1986: Toward atmospheres without tops: Absorbing upper boundary conditions for numerical models. *Quart. J. Roy. Meteor. Soc.,* **112,** 1195–1218.

——, and D. L. Williamson, 1990: Computational aspects of moisture transport in global models of the atmosphere. *Quart. J. Roy. Meteor. Soc.,* **116,** 1071–1090.

——, and ——, 1991: Sensitivity of a general circulation model climate to the moisture transport formulation. *J. Geophys. Res.,* **96,** 13 123–13 137.

——, B. A. Boville, and G. P. Brasseur, 1995: A three-dimensional general circulation model with coupled chemistry for the middle atmosphere. *J. Geophys. Res.,* **100,** 9041–9071.

——, and Coauthors, 2000: A comparison of scavenging and deposition processes in global models; Results from the WCRP Cambridge workshop of 1995. *Tellus,* **52B,** 1025–1056.

——, and Coauthors, 2006: Characterization of tropical transient activity in the CAM3 atmospheric hydrologic cycle. *J. Climate,* **19,** 2222–2242.

Ray, E. A., F. L. Moore, J. W. Elkins, G. S. Dutton, D. W. Fahey, H. Vmel, S. J. Oltmans, and K. H. Rosenlof, 1999: Transport into the northern hemisphere lowermost stratosphere revealed by in situ tracer measurements. *J. Geophys. Res.,* **104,** 26 565–26 580.

Rind, D., and J. Lerner, 1996: The use of online tracers as a diagnostic tool in GCM model development. *J. Geophys. Res.,* **101,** 12 667–12 683.

——, ——, K. Shah, and R. Suozzo, 1999: Use of online tracers as a diagnostic tool in general circulation model development, 2. transport between the troposphere and stratosphere. *J. Geophys. Res.,* **104,** 9151–9167.

——, ——, and C. McLinden, 2001: Changes of tracer distributions in the doubled CO2 climate. *J. Geophys. Res.,* **106,** 28 061–28 079.

Waugh, D. W., and T. M. Hall, 2002: Age of stratospheric air: Theory, observations and models. *Rev. Geophys.,* **40,** 1010, doi:10.1029/2000RG000101.

Williamson, D. L., 1983: Description of NCAR Community Climate Model (CCM0B). Tech. Rep. NCAR/TN-210+STR, National Center for Atmospheric Research, Boulder, CO, 88 pp.

——, and J. G. Olson, 1994: Climate simulations with a semi-Lagrangian version of the NCAR Community Climate Model. *Mon. Wea. Rev.,* **122,** 1594–1610.

——, and P. J. Rasch, 1994: Water vapor transport in the NCAR CCM2. *Tellus,* **46A,** 34–51.

——, and J. G. Olson, 1998: A comparison of semi-Lagrangian and Eulerian polar climate simulations. *Mon. Wea. Rev.,* **126,** 991–1000.

Zeng, G., and J. A. Pyle, 2003: Changes in tropospheric ozone between 2000 and 2100 modeled in a chemistry-climate model. *Geophys. Res. Lett.,* **30,** 1392, doi:10.1029/2002GL016708.